

[Click here to view linked References](#)

Title page

DEVELOPMENT OF A TRANSPLANTABLE GLIOMA TUMOUR MODEL FROM GENETICALLY ENGINEERED MICE. MRI/MRS/MRSI CHARACTERISATION

Magdalena Ciezka ^{1,2}, Milena Acosta ^{1,2}, Cristina Herranz ^{3,4,5,6}, Josep M. Canals ^{3,4,5,6}, Martí
Pumarola ^{8,2}, Ana Paula Candiota ^{2,1,7§}, Carles Arús ^{1,2,7}.

1. Departament de Bioquímica i Biologia Molecular, Unitat de Bioquímica de Biociències, Edifici Cs, Universitat Autònoma de Barcelona, 08193, Cerdanyola del Vallès, Spain.
2. Centro de Investigación Biomédica en Red en Bioingeniería, Biomateriales y Nanomedicina (CIBERBBN), Spain.
3. Laboratory of Stem Cells and Regenerative Medicine, Department of Biomedical Sciences, Faculty of Medicine and Health Sciences, University of Barcelona, Barcelona, SPAIN.
4. Research and Development Unit, Cell Therapy Program, Faculty of Medicine and Health Sciences, University of Barcelona, Barcelona, SPAIN.
5. Institut d'Investigacions Biomèdiques August Pi i Sunyer, Barcelona, SPAIN.
6. Centro de Investigación Biomédica en Red sobre Enfermedades Neurodegenerativas (CIBERNED), SPAIN
7. Institut de Biotecnologia i de Biomedicina, Universitat Autònoma de Barcelona, 08193, Cerdanyola del Vallès, Spain.
8. Departament de Medicina i Cirurgia Animals, Facultat de Veterinària, Edifici V, Universitat Autònoma de Barcelona, 08193 Bellaterra (Cerdanyola del Vallès), Barcelona, Spain

§Corresponding author

Email: AnaPaula.Candiota@uab.cat

Phone number: +34 93 5814126

Fax number: +34 93 5811264

Acknowledgements

Post-print of: Ciezka, M, et al. "Development of a transplantable glioma tumour model from genetically engineered mice: MRI/MRS/MRSI characterisation" in Journal of neuro-oncology (Springer). Published online June 2016. The final version is available at DOI 10.1007/s11060-016-2164-3

1 This work was funded by the Ministerio de Economía y Competitividad (MINECO) grants MARESCAN
2 (SAF 2011-23870), MOLIMAGLIO (SAF2014-52332-R) and SAF2012-37417. Also funded by the
3
4 ISCiii-Subdirección General de Evaluación and European Regional Development Fund (ERDF) [RETICS
5 to JMC (RD12/0019/0002; Red de Terapia Celular)], Spain, and by Centro de Investigación Biomédica
6 en Red – Bioingeniería, Biomateriales y Nanomedicina (CIBER-BBN, [<http://www.ciber-bbn.es/en>]), an
7
8 initiative of the Instituto de Salud Carlos III (Spain) co-funded by EU Fondo Europeo de Desarrollo
9
10 Regional (FEDER).
11
12

13 M. Ciezka held an FI-DGR predoctoral fellowship (FI-DGR 2012) from the Generalitat de Catalunya.
14

15 M. Ciezka and M. Acosta contributed equally to data acquisition.
16
17
18
19
20
21
22
23
24
25
26
27
28
29
30
31
32
33
34
35
36
37
38
39
40
41
42
43
44
45
46
47
48
49
50
51
52
53
54
55
56
57
58
59
60
61
62
63
64
65

ABSTRACT

Objective. The initial aim of this study was to generate a transplantable glial tumour model of low-intermediate grade by disaggregation of a spontaneous tumour mass from genetically engineered mice (GEM). This should result in an increased tumour incidence in comparison to GEM animals. *Methods.* An anaplastic oligoastrocytoma (OA) tumour of WHO grade III was obtained from a female GEM mouse with the S100 β -v-erbB/inK4a-Arf (+/-) genotype maintained in the C57BL/6 background. The tumour tissue was disaggregated; tumour cells from it were grown in aggregates and stereotactically injected into C57BL/6 mice. Tumour development was followed using Magnetic Resonance Imaging (MRI), while changes in the metabolomics pattern of the masses were evaluated by Magnetic Resonance Spectroscopy/Spectroscopic Imaging (MRS/MRSI). Final tumour grade was evaluated by histopathological analysis. *Results.* The total number of tumours generated from GEM cells from disaggregated tumour (CDT) was 67 with up to 100% penetrance, as compared to 16% in the local GEM model, with an average survival time of 66 \pm 55 days, up to 4.3-fold significantly higher than the standard GL261 glioblastoma (GBM) tumour model. Tumours produced by transplantation of cells freshly obtained from disaggregated GEM tumour were diagnosed as WHO grade III anaplastic oligodendroglioma (ODG) and OA, while tumours produced from a previously frozen sample were diagnosed as WHO grade IV GBM. *Conclusions.* We successfully grew CDT and generated tumours from a grade III GEM glial tumour. Freezing and cell culture protocols produced progression to grade IV GBM, which makes the developed transplantable model qualify as potential secondary GBM model in mice.

KEYWORDS

Preclinical Brain Tumour, Molecular Imaging, Secondary Glioblastoma, Disaggregated Tumour

ABBREVIATION LIST

BBB, Blood-brain barrier; CDT, Cells from disaggregated tumour; CE, Contrast-enhanced; Cho, Choline; Cr, Creatine; DCE, Dynamic contrast enhancement; DMSO, Dimethyl sulfoxide; FASTMAP, Fast Automatic Shimming Technique By Mapping Along Projections; GABRMN, Grup d'Aplicacions Biomèdiques de la Resonància Magnètica Nuclear; GBM, Glioblastoma; GEM, Genetically engineered mice; GFAP, Glial fibrillary acid protein; Glc, D-glucose; ip, intraperitoneal; IST, inter-slice thickness; KO, knocked out; Lac, Lactate; LET, Long echo time; ML, Mobile lipids; MR, Magnetic Resonance;

1 MRI, Magnetic Resonance Imaging; MRS, Magnetic Resonance Spectroscopy; MRSI, Magnetic
2 Resonance Spectroscopic Imaging; NA, Number of averages; NAA, N-acetylaspartate; OA,
3 Oligoastrocytoma; ODG, Oligodendroglioma; Olig2, Oligodendrocyte transcription factor; PBS,
4 Phosphate Buffered Saline; PCR, Polymerase chain reaction; PE-MRSI, Perturbation enhanced MRSI;
5 p.i., Post-implantation; PR, Pattern recognition; PRESS, Point-resolved spectroscopy; RARE, Rapid
6 Acquisition with Relaxation Enhancement; SD, Standard deviation; SET, Short echo time; spv, spectral
7 vector; ST, Slice thickness; SV, Single voxel, TAT, Total Acquisition Time; Tau, Taurine; TE, Echo
8 Time; TR, Recycling Time; UL, Unit Length; VAPOR, Variable pulse power and optimized relaxation
9 delays; VOI, Volume of interest; WHO World Health Organization

19 INTRODUCTION

21 Gliomas are one of the most life threatening and the most common primary human brain
22 malignancies with annual incidence of ~5 cases per 100,000 people [1,2]. Despite advancements in
23 surgery and adjuvant therapy, the prognosis remains very poor, with a median survival of less than 15
24 months for glioblastoma (GBM) [3], and 3-7 years for anaplastic glial tumours [4-6].

29 Improvement of diagnosis and therapeutics requires reliable animal glioma models, and many
30 have been developed for this purpose. They can be divided into genetically engineered models (GEM)
31 and engrafted tumour models. GEMs allow recapitulating specific genetic patterns of primary human
32 glioma [7,8]. However, late and stochastic onset and the inherent difficulty to detect brain masses in a
33 timely fashion make them impractical for therapy response studies [9]. Additionally, the incidence of
34 GEM tumours may be smaller than incidence achieved in transplantable models [7,10,11] and may vary
35 with time or with crosses because of genetic background problems, while the stereotactic injection models
36 maintain almost full penetrance. Due to high penetrance and reproducible tumour growth, the engrafted
37 models are the most used for evaluating new therapies for glioma. To combine advantages of both
38 models, transplantable models derived from GEM have been used [12,13].

49 *In vivo* characterisation and monitoring of brain tumours, alongside with development of new
50 cancer models, is of major importance for progression or therapy response studies. In this respect,
51 Magnetic Resonance Imaging (MRI) is the most used technique for diagnosis and management of brain
52 tumours, providing detailed anatomic information [14,15]. This can be supported by Magnetic Resonance
53 Spectroscopy (MRS) and Spectroscopic Imaging (MRSI), which allow collecting non-invasive
54 biomarkers, that may provide important clues about tumour biology and response to treatment [16,17].

1
2
3
4
5
6
7
8
9
10
11
12
13
14
15
16
17
18
19
20
21
22
23
24
25
26
27
28
29
30
31
32
33
34
35
36
37
38
39
40
41
42
43
44
45
46
47
48
49
50
51
52
53
54
55
56
57
58
59
60
61
62
63
64
65

Single voxel (SV) MRS measures the average metabolic information of a tumour [16,17], whereas multivoxel acquisition (MRSI) provides spatially resolved metabolic information [18-20], which may be superimposed to anatomical acquisitions. Additionally, our group has developed MRSI-based molecular imaging techniques, perturbing the spectral pattern (Perturbation Enhanced Magnetic Resonance Spectroscopic Imaging, PE-MRSI) by injecting different substances, such as dimethyl sulfoxide (DMSO) and glucose [21-23], to increase the dynamic range for *in vivo* preclinical brain tumour characterization.

In this work we have attempted to establish a low/intermediate grade transplantable glioma model by disaggregation of a GEM brain mass and to characterise this tumour model through magnetic resonance techniques.

MATERIALS AND METHODS

GL261 cell culture

The murine GL261 glioma cell line was obtained from the Tumour Bank Repository at the National Cancer Institute (Frederick/MD, USA). Cells were grown as previously described [22].

Animals

A total of 86 C57BL/6 female mice of 18-24g in weight, aged 16-20 weeks, obtained from Charles River Laboratories (Charles River Laboratories International, L'Arbresle, France), were used in this study.

Founders for the GEM colony (S100 β -v-erbB/inK4a-Arf (+/-) genotype maintained in the C57BL/6 background) were obtained through the Mouse Models of Human Cancer Consortium Repository at the National Cancer Institute (MMHCC-NCI, Frederick, MD, USA) [24]. A spontaneous tumour developed in a GEM mouse, diagnosed as anaplastic OA (details in results section), was used to grow the culture of cells from disaggregated tumour (CDT).

All mice were housed in the animal facility of Universitat Autònoma de Barcelona (Servei d'Estabulari). Studies were approved by the local ethics committee (protocols CEEAH 1176 and 2449).

CDT culture

Mice were sacrificed by cervical dislocation, and tumours were excised and disaggregated mechanically with a fire-polished Pasteur pipette. CDT were grown as aggregates and some CDT aggregates were frozen to check the reliability and repeatability of cultured cells for transplantation purposes. CDT culture conditions are described in the Supplementary Material file.

Tumour generation

1 C57BL/6 mice (n=86) were divided into 6 groups (summarized in Supplementary Table 1). For
2 set-up studies with GL261 tumours, 19 animals were used: 6 animals implanted with GL261 cells for
3 standard GBM generation (group A); 13 animals injected with CDT cultured from GL261 tumours from
4 “A” group (6 from fresh and 7 from tumour frozen in liquid N₂ for 6 months, groups B and C
5 respectively). For GEM tumour studies, 67 animals were used: 29 animals (group D) implanted with CDT
6 cultured from the freshly extracted S912 tumour (referred to as fresh CDT); a further group of 29 animals
7 (group E) implanted with CDT obtained from S912 tumour, in which CDT aggregates were frozen in
8 liquid N₂ during 5 months, thawed and recultured prior to implantation (referred to as frozen CDT); and
9 finally, 9 mice implanted with CDT obtained from a frozen piece of S912 tumour (group F). .
10
11
12
13
14
15
16
17

18 Tumours were induced in mice as previously reported [22], either from GL261 cultured cells or
19 CDT. In case of tumours generated from fresh CDT, cells were not counted before implantation, but it
20 was assumed that each well of the multi-well plate contained ~10⁵, considering cell counting before
21 seeding and their assumed proliferation rate.
22
23
24
25

26 **MR studies**

27
28 All MR studies were performed at UNIT 25 of NANBIOSIS, a joint NMR facility of the
29 Universitat Autònoma de Barcelona and CIBER-BBN (Cerdanyola del Vallès, Spain). The
30 MRI/MRS/MRSI sequences and MR data post-processing are detailed in the Supplementary Material file.
31
32 Briefly, coronal high resolution T_{2w} images were acquired every 3-6 days during the first month of
33 tumour evolution, starting on day 9 post-implantation (p.i.), and every 15 days thereafter if a mass was
34 not detected. SV spectra were acquired at short and long echo time. Tumour-bearing mice were also
35 studied by PE-MRSI with DMSO [21] and/or with glucose under mild hypothermia [22,23]. Blood brain
36 barrier (BBB) integrity was evaluated with gadoterate meglumine (DOTAREM, Guerbet, Roissy, France)
37 using contrast-enhanced (CE) T_{1w} images.
38
39
40
41
42
43
44
45

46 **Tissue preservation for post-mortem procedures**

47
48 *In vivo* MR studies and tumour progression follow up took place until animals died or were
49 sacrificed, due to animal welfare protocol, by cervical dislocation. The brains of 49 mice were excised
50 and fixed in 4% formaldehyde. Further details are described in the Supplementary Material file.
51
52
53

54 **Genotype check**

55
56 Transgene presence and knock-out mutations of the GEM S912 mouse and selected S912-
57 derived tumours were checked by polymerase chain reaction (PCR) analysis performed on DNA
58
59
60
61
62
63
64
65

1 extractions from a piece of tail or tumour, respectively. Technical details can be found at Supplementary
2 Material file.

3 **Statistics**

4 Detailed information about statistical tests can be found in the Supplementary Material file.
5
6

7 **RESULTS**

8 **Passage of tumours obtained from disaggregation of GL261 GBM**

9
10
11
12
13
14
15
16
17
18
19
20
21
22
23
24
25
26
27
28
29
30
31
32
33
34
35
36
37
38
39
40
41
42
43
44
45
46
47
48
49
50
51
52
53
54
55
56
57
58
59
60
61
62
63
64
65
GL261 tumour-bearing mice were sacrificed once masses reached a volume of 140 ± 20 mm³ (n=6, day 18 ± 2 p.i.) and tumour tissue was used for CDT culture (Supplementary Figure 1A).

Tumours developed from CDT of fresh GL261 GBM were detectable by MRI on day 8 p.i., while tumours grown from CDT obtained from frozen GL261 GBM were detectable on day 10 p.i., resulting in a slightly longer survival than the group implanted with freshly disaggregated tumours. Both achieved full penetrance. Further details on volumes and survival can be found in the Supplementary Material file (Supplementary Results section and Supplementary Figure 2, as well as Supplementary Table 2, respectively).

66 **Generation of tumours from CDT obtained from S912 GEM**

The MRI screening of the GEM colony [25,26] detected a brain mass in the S912 mouse (S912 being a unique alphanumeric identifier for animals in our research group), female, by 14 weeks of age, with the S100 β -v-erbB transgene and heterozygotic KO for inK4a-Arf (+/-) [7]. The T_{2w} images 32 days after the initial detection showed a circumscribed mass (about 22 mm³ in volume) in the rostral diencephalon (Supplementary Figure 3A). The CE-MRI T_{1w} studies (Supplementary Figure 3B-3C) showed a partially disrupted BBB, indicating an heterogeneous mass. The histopathological diagnosis at day 61 post detection was anaplastic OA - of WHO grade III (please check Supplementary Figure 4 for further details). Supplementary Figure 1B shows CDT aggregates cultured from this freshly resected tumour.

67 *MRI assessment of tumour growth and penetrance estimation*

68 *Fresh CDT*

Mice implanted with fresh CDT had 55% of tumour incidence during the monitoring period of 3 months. Masses showed two distinct growth patterns and were classified into two groups: 'short latency' (evolution similar to GL261 CDT tumours) and 'intermediate latency' (delayed detection (25 ± 33 days)

1
2
3
4
5
6
7
8
9
10
11
12
13
14
15
16
17
18
19
20
21
22
23
24
25
26
27
28
29
30
31
32
33
34
35
36
37
38
39
40
41
42
43
44
45
46
47
48
49
50
51
52
53
54
55
56
57
58
59
60
61
62
63
64
65

with respect to GL261 CDT tumours (day 8)). An arbitrary cut-off boundary at 16 days was chosen for this. Table 1 summarises average time of first detection and final tumour volume.

Frozen CDT

All animals of this group developed masses with detection spread out in time, having a more irregular appearance (Figure 1B and 1C) in comparison to those generated by GL261 cells or fresh S912 CDT. Most masses were detected between day 14 and 21 p.i., although some tumours were detected much later, after 8 months p.i. Tumour doubling time also varied, as in the group implanted with fresh CDT (Table 1). As previously, animals were divided into different groups based on tumour growth kinetics - ‘short latency’, ‘intermediate latency’ and an additional ‘long latency’ group. In the ‘intermediate latency’ group, some tumours did not show detectable volume increase for extended periods of time (e.g. 10 weeks for the Gc15-S912 mouse) until they started growing again. ‘Long latency’ refers to masses detected not earlier than day 53 p.i. and tumour evolution ranging between 12–29 days after then.

Masses from the ‘intermediate’ and ‘long latency’ groups tended to grow in or associated to ventricles (Figure 1D), and this also applies to frozen S912 tumour-derived masses.

CDT obtained from frozen tumour

The evolution of tumours from this group mostly resembled the GL261 standard tumours growth pattern (Table 1 and reference [27]), apart from two animals: one developed an ‘intermediate latency’ tumour type and another one a ‘long latency’ tumour type (detection at day 80 p.i.). Tumour incidence was 100%, and in most mice, the initial mass was detectable by T_{2w} MRI on the day 10 p.i.

MRS

Details about MRS results showing correlation between peak height ratios and tumour growth/progression can be found in Supplementary Tables 3 and 4.

MRSI

Data from PE-MRSI using DMSO were used to produce maps of differential DMSO accumulation. Figure 2A-D illustrates an example of the ‘short latency’ group, showing that DMSO accumulates essentially in the internal area of the tumour. At this time point, the tumour had intact BBB (Figure 2E), compatible with low-intermediate grade characteristics.

Pattern recognition

1
2
3
4
5
6
7
8
9
10
11
12
13
14
15
16
17
18
19
20
21
22
23
24
25
26
27
28
29
30
31
32
33
34
35
36
37
38
39
40
41
42
43
44
45
46
47
48
49
50
51
52
53
54
55
56
57
58
59
60
61
62
63
64
65

Pattern recognition analysis was used to classify voxels from the glucose-perturbed MRSI matrices from normal brain parenchyma, ODG (grade II) or GBM (grade IV) using the classifier available at our group for this discrimination [28]. Nosological maps for two mice are presented in Figure 3. The MSRI based classifier for tumour G1-S912 on day 39 p.i. shows an heterogeneous pattern compatible with transition between grade II, with ODG component, and grade IV. As this classifier did not contain grade III class cases, the classification could suggest an heterogeneous high grade glioma with oligodendroglial component. Histopathology for G1-S912 was anaplastic oligodendroglioma (WHO grade III). BBB status was still intact on day 28 p.i. (not shown). For tumour Gc26-S912 (day 35 p.i.) the PE-MRSI pattern and nosological image indicated a GBM, which was indeed the final histopathology diagnostic.

Survival

The survival of each group is shown in Figure 4 and Supplementary Table 2. Significant differences ($p \leq 0.05$) in survival of mice implanted with CDT from S912 tumour were found in comparison with animals implanted with either cultured GL261 cells or GL261 CDT. Up to a 4.3-fold increase in the standard GL261 average survival was found.

Histopathology Studies

The original S912 tumour, as well as 48 out of 54 tumours generated from it, underwent histopathological analysis. From the 16 animals with tumours developed from fresh CDT, 12 were diagnosed as grade III: 8 anaplastic ODGs and 4 OAs (see Supplementary Results and *Histopathology Studies* section for histopathological descriptions). The remaining 4 tumours were saved for future CDT culture/transplantation, and no histopathological analysis has been performed. The diagnosis for 27 out of 29 animals implanted with frozen CDT and for all 9 mice implanted with CDT from frozen S912 tumour showed clear progression, being classified as grade IV GBM. Samples of two animals could not undergo histopathological analysis due to insufficient tissue integrity.

Genotype check

Detailed results/discussion for the genotype assessment can be found in *Genotype check* sections in Supplementary Results and Supplementary Discussion).

DISCUSSION

Disaggregated tumour model using CDT from GL261

1 The GL261 murine glioma was used for optimization studies because it is a well characterised
2 model with reproducible growth pattern [11,23]. The disaggregation technique of solid tumour tissue has
3 been widely used for establishment of new glioma cell lines [29]. In this work, GL261 CDT were cultured
4 and, upon implantation, resulting similar to the standard GL261 tumour model regarding penetrance,
5 growth pattern and survival time (Supplementary Figure 2 and Supplementary Table 2). This is in
6 agreement with studies that produced “neurospheres” from cultured GL261 cells and did not find
7 significant differences in survival time between animals implanted with 5×10^4 cells from GL261
8 “neurospheres” (23.4 ± 4.6 days) and those implanted with the same amount of GL261 cells directly from
9 cell culture (29.8 ± 6.4 days) [30]. However, when the concentration of the inoculum used decreased, cells
10 from “neurospheres” confirmed a more aggressive behaviour with significantly reduced survival time.
11 This was not studied in our case.
12
13
14
15
16
17
18
19
20
21

22 Additionally, our results proved that culture of CDT from a frozen GL261 mass was also
23 feasible, reaching full tumour penetrance. This finding is in line with studies demonstrating that using
24 frozen tissue for establishment of stable outgrowing cells does not significantly decrease take rates in
25 comparison to fresh material [31]. This should be useful, as it is not always possible to work with freshly
26 excised masses. Still, authors in [31] did not evaluate performance in allograft transplantation
27 experiments.
28
29
30
31
32
33

34 *Disaggregated tumour model from a GEM anaplastic OA: S912 tumour*

35 Applying the optimized method to a GEM fresh tumour showed a penetrance of 55% in
36 comparison to ~90% for spontaneous tumour development described by providers [7], but clearly higher
37 than penetrance found in our lab ($\approx 16\%$, [25,26]). This penetrance was also much lower than 96% for the
38 standard GL261 model (GABRMN unpublished results, $n=832$) or full penetrance in GL261 setup
39 experiments from this work ($n=6$). When repeating studies with frozen CDT from GEM or frozen GEM
40 tumour, the penetrance increased to 100%. A possible explanation for this would be that culturing,
41 freezing, thawing and growing helps selecting for a more aggressive cellular subtype, possibly
42 accumulating additional mutations, favouring higher grade tumours development. This would be in line
43 with literature, which describes that it is difficult to obtain a low/intermediate grade stable cell line. Thus,
44 Shimada et al. [32] showed that aggressive tumours allow to establish stable cell lines from primary
45 culture, while it proves difficult with non-aggressive tumours. Authors in [32] also suggested that the
46 mutational status of p53 and MDM2 plays an important role in development of stable tumoural cell lines
47
48
49
50
51
52
53
54
55
56
57
58
59
60
61
62
63
64
65

1
2
3
4
5
6
7
8
9
10
11
12
13
14
15
16
17
18
19
20
21
22
23
24
25
26
27
28
29
30
31
32
33
34
35
36
37
38
39
40
41
42
43
44
45
46
47
48
49
50
51
52
53
54
55
56
57
58
59
60
61
62
63
64
65

for tumour generation. Other authors have reported that expansion of tumour cells via *in vitro* culture can affect the characteristics of developed masses in comparison with the original tumour. In this respect, Barker et al. [33], after 6 months of cell culture, observed that implanted tumours originally diagnosed as astrocytoma with anaplastic features (grade III), were later classified as mixed GBM/sarcoma or gliosarcoma (grade IV). Halfter et al. [34] established cell lines from a mixed oligoastrocytoma and an astrocytoma, both of grade II/III, and only the latter induced tumour in athymic mice. Onda et al. [35] established glioma cell lines from two surgical specimens obtained from the same patient at different times; one was derived from the primary tumour (slightly anaplastic astrocytoma, grade II/III), while another was from the recurrent tumour (GBM, grade IV) and subcutaneous tumours developed only after inoculation of the higher grade cells into nude mice. However, in contrast to what was described in [32], neither of the cell lines generated in [35] had alteration in p53 mutational status.

On the other hand, it has been reported that cryopreserved human “spheroids” retain their histological characteristics after thawing [36] and when xenografted into nude mice after defreezing, their essential phenotypic traits and gene expression profiles do not change significantly [37,38]. However, “spheroids” reported in both studies were originally derived from GBM, already grade IV tumour. Therefore, further work is needed to clarify the cause of the recorded progression in our case, and the mutational status of driver genes may need to be evaluated.

Additionally, survival of animals in nearly all groups implanted with CDT from S912 was larger than for the GL261 model (Supplementary Table 2). There was a significant difference between S912 tumours derived from fresh CDT and tumours derived from fresh GL261 CDT, as well as between frozen CDT long latency group tumours and fresh S912 CDT derived tumours, which may be of interest for therapy response studies in our group [27].

Non-invasive MR monitoring of S912 CDT-derived tumours

The MRI/MRS/MRSI acquisition of S912-derived tumours allowed *in vivo* assessment of their grade, later confirmed by histopathology. A discussion about MRS results can be found in the Supplementary Material file. The PE-MRSI derived classifier allowed non-invasive evaluation of tumours. Tumours derived from fresh S912 CDT were classified as ODG or mixed ODG/GBM, pointing to heterogeneous tumours with transition regions from grade II/III to grade IV. A classifier incorporating grade III cases would have been required, but it is not yet available. On the other hand, most of tumours from groups E and F were classified as GBM, in line with their histopathological diagnosis.

1
2
3
4
5
6
7
8
9
10
11
12
13
14
15
16
17
18
19
20
21
22
23
24
25
26
27
28
29
30
31
32
33
34
35
36
37
38
39
40
41
42
43
44
45
46
47
48
49
50
51
52
53
54
55
56
57
58
59
60
61
62
63
64
65

Furthermore, the information obtained from PE-MRSI with DMSO could be useful for those developing new transplantable models for preclinical studies. DMSO is confirmed to serve as a contrast agent for early brain tumour detection (Figure 3), independent of their BBB integrity as already proposed [21]. This could be useful for therapy monitoring and for evaluating non-invasively local heterogeneities associated with progression or therapy response [27], something anatomic MRI alone cannot provide [39]. Further studies are needed in order to validate these findings with histopathological features associated with tumour relapse/response.

Conclusions

We successfully established a new transplantable model of GBM with significantly slower growth and higher survival time with respect to the standard GL261 model, and with significantly higher penetrance than the original GEM colony. The fact that the S912 mass, used for CDT culture, was originally diagnosed as anaplastic OA (grade III) and that the procedures related to CDT culture generation, freezing and transplantation produced a progression to grade IV GBM, makes the developed transplantable model qualify as a potential secondary GBM model, which may be of interest in future therapy monitoring protocols.

References

1. Louis DN, Ohgaki H, Wiestler OD, Cavenee WK, Burger PC, Jouvet A, Scheithauer BW, Kleihues P (2007) The 2007 WHO classification of tumours of the central nervous system. *Acta Neuropathol* 114 (2):97-109. doi:10.1007/s00401-007-0243-4
2. Ostrom QT, Gittleman H, Farah P, Ondracek A, Chen Y, Wolinsky Y, Stroup NE, Kruchko C, Barnholtz-Sloan JS (2013) CBTRUS statistical report: Primary brain and central nervous system tumors diagnosed in the United States in 2006-2010. *Neuro-oncology* 15 Suppl 2:ii1-56. doi:10.1093/neuonc/not151
3. Stupp R, Mason WP, van den Bent MJ, Weller M, Fisher B, Taphoorn MJ, Belanger K, Brandes AA, Marosi C, Bogdahn U, Curschmann J, Janzer RC, Ludwin SK, Gorlia T, Allgeier A, Lacombe D, Cairncross JG, Eisenhauer E, Mirimanoff RO (2005) Radiotherapy plus concomitant and adjuvant temozolomide for glioblastoma. *The New England journal of medicine* 352 (10):987-996. doi:10.1056/NEJMoa043330
4. Nieder C, Grosu AL, Mehta MP, Andratschke N, Molls M (2004) Treatment of malignant gliomas: radiotherapy, chemotherapy and integration of new targeted agents. *Expert review of neurotherapeutics* 4 (4):691-703. doi:10.1586/14737175.4.4.691
5. Prados MD, Seiferheld W, Sandler HM, Buckner JC, Phillips T, Schultz C, Urtasun R, Davis R, Gutin P, Cascino TL, Greenberg HS, Curran WJ, Jr. (2004) Phase III randomized study of radiotherapy plus procarbazine, lomustine, and vincristine with or without BUdR for treatment of anaplastic astrocytoma: final report of RTOG 9404. *International journal of radiation oncology, biology, physics* 58 (4):1147-1152. doi:10.1016/j.ijrobp.2003.08.024
6. van den Bent MJ, Carpentier AF, Brandes AA, Sanson M, Taphoorn MJ, Bernsen HJ, Frenay M, Tijssen CC, Grisold W, Sipos L, Haaxma-Reiche H, Kros JM, van Kouwenhoven MC, Vecht CJ, Allgeier A, Lacombe D, Gorlia T (2006) Adjuvant procarbazine, lomustine, and vincristine improves progression-free survival but not overall survival in newly diagnosed anaplastic oligodendrogliomas and oligoastrocytomas: a randomized European Organisation for Research and Treatment of Cancer phase III trial. *Journal of clinical oncology : official journal of the American Society of Clinical Oncology* 24 (18):2715-2722. doi:10.1200/JCO.2005.04.6078
7. Weiss WA, Burns MJ, Hackett C, Aldape K, Hill JR, Kuriyama H, Kuriyama N, Milshteyn N, Roberts T, Wendland MF, DePinho R, Israel MA (2003) Genetic determinants of malignancy in a mouse model for oligodendroglioma. *Cancer research* 63 (7):1589-1595
8. Hu X, Pandolfi PP, Li Y, Koutcher JA, Rosenblum M, Holland EC (2005) mTOR promotes survival and astrocytic characteristics induced by Pten/AKT signaling in glioblastoma. *Neoplasia* 7 (4):356-368
9. Alcoser SY, Hollingshead MG (2011) Genetically Engineered Mouse Models in Preclinical Anti-Cancer Drug Development. In: Kapetanović I (ed) *Drug Discovery and Development - Present and Future*. InTech, Available from: <http://www.intechopen.com/books/drug-discovery-and-development-present-and-future/genetically-engineered-mouse-models-in-preclinical-anti-cancer-drug-development>. Last accessed 28/12/2015. doi:10.5772/30666
10. Cha S, Johnson G, Wadghiri YZ, Jin O, Babb J, Zagzag D, Turnbull DH (2003) Dynamic, contrast-enhanced perfusion MRI in mouse gliomas: correlation with histopathology. *Magnetic resonance in medicine : official journal of the Society of Magnetic Resonance in Medicine / Society of Magnetic Resonance in Medicine* 49 (5):848-855. doi:10.1002/mrm.10446
11. Szatmari T, Lumniczky K, Desaknai S, Trajcevski S, Hidvegi EJ, Hamada H, Safrany G (2006) Detailed characterization of the mouse glioma 261 tumor model for experimental glioblastoma therapy. *Cancer science* 97 (6):546-553. doi:10.1111/j.1349-7006.2006.00208.x
12. Smilowitz HM, Weissenberger J, Weis J, Brown JD, O'Neill RJ, Laissue JA (2007) Orthotopic transplantation of v-src-expressing glioma cell lines into immunocompetent mice: establishment of a new transplantable in vivo model for malignant glioma. *Journal of neurosurgery* 106 (4):652-659. doi:10.3171/jns.2007.106.4.652

13. El Meskini R, Iacovelli AJ, Kulaga A, Gumprecht M, Martin PL, Baran M, Householder DB, Van Dyke T, Weaver Ohler Z (2015) A preclinical orthotopic model for glioblastoma recapitulates key features of human tumors and demonstrates sensitivity to a combination of MEK and PI3K pathway inhibitors. *Dis Model Mech* 8 (1):45-56. doi:10.1242/dmm.018168
14. Borges AR, Lopez-Larrubia P, Marques JB, Cerdan SG (2012) MR imaging features of high-grade gliomas in murine models: how they compare with human disease, reflect tumor biology, and play a role in preclinical trials. *AJNR American journal of neuroradiology* 33 (1):24-36. doi:10.3174/ajnr.A2959
15. Brandes AA, Tosoni A, Franceschi E, Reni M, Gatta G, Vecht C (2008) Glioblastoma in adults. *Critical reviews in oncology/hematology* 67 (2):139-152. doi:10.1016/j.critrevonc.2008.02.005
16. Majos C, Alonso J, Aguilera C, Serrallonga M, Perez-Martin J, Acebes JJ, Arus C, Gili J (2003) Proton magnetic resonance spectroscopy ((1)H MRS) of human brain tumours: assessment of differences between tumour types and its applicability in brain tumour categorization. *Eur Radiol* 13 (3):582-591. doi:10.1007/s00330-002-1547-3
17. Sibtain NA, Howe FA, Saunders DE (2007) The clinical value of proton magnetic resonance spectroscopy in adult brain tumours. *Clin Radiol* 62 (2):109-119. doi:10.1016/j.crad.2006.09.012
18. Martinez-Bisbal MC, Celda B (2009) Proton magnetic resonance spectroscopy imaging in the study of human brain cancer. *Q J Nucl Med Mol Imaging* 53 (6):618-630. doi:R39092218 [pii]
19. Nelson SJ, Graves E, Pirzkall A, Li X, Antiniw Chan A, Vigneron DB, McKnight TR (2002) In vivo molecular imaging for planning radiation therapy of gliomas: an application of 1H MRSI. *J Magn Reson Imaging* 16 (4):464-476. doi:10.1002/jmri.10183
20. Nelson SJ, Vigneron DB, Dillon WP (1999) Serial evaluation of patients with brain tumors using volume MRI and 3D 1H MRSI. *NMR Biomed* 12 (3):123-138. doi:10.1002/(SICI)1099-1492(199905)12:3<123::AID-NBM541>3.0.CO;2-Y [pii]
21. Delgado-Goni T, Martin-Sitjar J, Simoes RV, Acosta M, Lope-Piedrafita S, Arus C (2013) Dimethyl sulfoxide (DMSO) as a potential contrast agent for brain tumors. *NMR Biomed* 26 (2):173-184. doi:10.1002/nbm.2832
22. Simoes RV, Garcia-Martin ML, Cerdan S, Arus C (2008) Perturbation of mouse glioma MRS pattern by induced acute hyperglycemia. *NMR Biomed* 21 (3):251-264. doi:10.1002/nbm.1188
23. Simoes RV, Delgado-Goni T, Lope-Piedrafita S, Arus C (2010) 1H-MRSI pattern perturbation in a mouse glioma: the effects of acute hyperglycemia and moderate hypothermia. *NMR Biomed* 23 (1):23-33. doi:10.1002/nbm.1421
24. https://mouse.ncifcrf.gov/available_details.asp?ID=01XD3. Last accessed: 28/12/2015.
25. Acosta M (2013) Mejora de los modelos preclínicos de tumores cerebrales. Aplicación a la caracterización ex vivo e in vivo de agentes de contraste nanoparticulados para imagen de resonancia magnetica. Universitat Autònoma de Barcelona, Available from: <http://hdl.handle.net/10803/128995>. Last accessed 28/12/2015
26. Ciezka M (2015) Improvement of protocols for brain cancer diagnosis and therapy response monitoring using magnetic resonance based molecular imaging strategies. Universitat Autònoma de Barcelona.
27. Delgado-Goni T, Julia-Sape M, Candiota AP, Pumarola M, Arus C (2014) Molecular imaging coupled to pattern recognition distinguishes response to temozolomide in preclinical glioblastoma. *NMR Biomed* 27 (11):1333-1345. doi:10.1002/nbm.3194
28. Simoes RV, Ortega-Martorell S, Delgado-Goni T, Le Fur Y, Pumarola M, Candiota AP, Martin J, Stoyanova R, Cozzone PJ, Julia-Sape M, Arus C (2012) Improving the classification of brain tumors in mice with perturbation enhanced (PE)-MRSI. *Integrative biology : quantitative biosciences from nano to macro* 4 (2):183-191. doi:10.1039/c2ib00079b
29. Masters JRW, Palsson B (2002) Human Cell Culture. Cancer cell lines. Kluwer Academic Publishers, New York (N.Y.)

- 1
2
3
4
5
6
7
8
9
10
11
12
13
14
15
16
17
18
19
20
21
22
23
24
25
26
27
28
29
30
31
32
33
34
35
36
37
38
39
40
41
42
43
44
45
46
47
48
49
50
51
52
53
54
55
56
57
58
59
60
61
62
63
64
65
30. Yi L, Zhou C, Wang B, Chen T, Xu M, Xu L, Feng H (2013) Implantation of GL261 neurospheres into C57/BL6 mice: a more reliable syngeneic graft model for research on glioma-initiating cells. *International journal of oncology* 43 (2):477-484. doi:10.3892/ijo.2013.1962
31. Mullins CS, Schneider B, Stockhammer F, Krohn M, Classen CF, Linnebacher M (2013) Establishment and characterization of primary glioblastoma cell lines from fresh and frozen material: a detailed comparison. *PloS one* 8 (8):e71070. doi:10.1371/journal.pone.0071070
32. Shimada Y, Maeda M, Watanabe G, Yamasaki S, Komoto I, Kaganoi J, Kan T, Hashimoto Y, Imoto I, Inazawa J, Imamura M (2003) Cell culture in esophageal squamous cell carcinoma and the association with molecular markers. *Clinical cancer research : an official journal of the American Association for Cancer Research* 9 (1):243-249
33. Barker M, Hoshino T, Gurcay O, Wilson CB, Nielsen SL, Downie R, Eliason J (1973) Development of an animal brain tumor model and its response to therapy with 1,3-bis(2-chloroethyl)-1-nitrosourea. *Cancer research* 33 (5):976-986
34. Halfter H, Kremerskothen J, Weber J, Hacker-Klom U, Barnekow A, Ringelstein EB, Stogbauer F (1998) Growth inhibition of newly established human glioma cell lines by leukemia inhibitory factor. *Journal of neuro-oncology* 39 (1):1-18
35. Onda K, Nagai S, Tanaka R, Morii K, Yoshimura JI, Tsumanuma I, Kumanishi T (1999) Establishment of two glioma cell lines from two surgical specimens obtained at different times from the same individual. *Journal of neuro-oncology* 41 (3):247-254
36. Goike HM, Asplund AC, Pettersson EH, Liu L, Ichimura K, Collins VP (2000) Cryopreservation of viable human glioblastoma xenografts. *Neuropathology and applied neurobiology* 26 (2):172-176
37. Sundlisaeter E, Wang J, Sakariassen PO, Marie M, Mathisen JR, Karlsen BO, Prestegarden L, Skaftnesmo KO, Bjerkvig R, Enger PO (2006) Primary glioma spheroids maintain tumorigenicity and essential phenotypic traits after cryopreservation. *Neuropathology and applied neurobiology* 32 (4):419-427. doi:10.1111/j.1365-2990.2006.00744.x
38. Chong YK, Toh TB, Zaiden N, Poonepalli A, Leong SH, Ong CE, Yu Y, Tan PB, See SJ, Ng WH, Ng I, Hande MP, Kon OL, Ang BT, Tang C (2009) Cryopreservation of neurospheres derived from human glioblastoma multiforme. *Stem cells* 27 (1):29-39. doi:10.1634/stemcells.2008-0009
39. Heiss WD, Raab P, Lanfermann H (2011) Multimodality assessment of brain tumors and tumor recurrence. *Journal of nuclear medicine : official publication, Society of Nuclear Medicine* 52 (10):1585-1600. doi:10.2967/jnumed.110.084210

TABLES

Table 1 Number of animals assigned into each group, time of initial tumour detection, average final volume and doubling time of masses

| Animal group | No of mice | Time of first mass detection by MRI (days p.i.) | Final volume (mm ³) ^a | Average doubling time (days) | |
|------------------------------|-----------------------------------|---|--|------------------------------|-------------|
| Standard GL261 | 6 | 6 | 195 ± 40.0 | 2.4 ± 0.3 | |
| Fresh GL261 CDT | 6 | 8 | 101 ± 26.0 | 2.1 ± 0.3 | |
| CDT from frozen GL261 tumour | 7 | 10 | 119 ± 32.0 | 2.3 ± 0.3 | |
| Fresh S912 CDT | Short latency ^d | 9 | 101.4 ± 58.9 | 4.3 ± 0.4 | |
| | Intermediate latency ^d | 7 | 25 ± 33 (between 16-97) | 181.0 ± 74.0 | 9.8 ± 12.1* |
| Frozen S912 CDT | Short latency | 13 | 15 ± 3 | 106.2 ± 59.4 | 3.4 ± 1.3 |
| | Intermediate latency | 9 | 21 ± 3 | 139.1 ± 71.2 ^b | 9.1 ± 2.8* |
| | Long latency ^d | 5 | 75 ± 104 (between 27-253) | 155.2 ± 50.1 | 9.5 ± 4.8* |
| CDT from frozen S912 tumour | 9 | 10 ± 3 ^c | 181.0 ± 74.0 | 3.5 ± 1.6 | |

^a This measure is a rough estimate, because some animals were screened before their death/sacrifice (up to 8 days)

^b Excluding Gc29-S912, because its last volume check was done 27 days before its death.

^c Excluding Gtc6-S912, in which the abnormal mass was only detected by MRI on the day 80 p.i.

^d See text for definition of 'short latency', 'intermediate latency' and 'long latency'

* There was a significant difference between intermediate/long latency and short latency groups

FIGURES

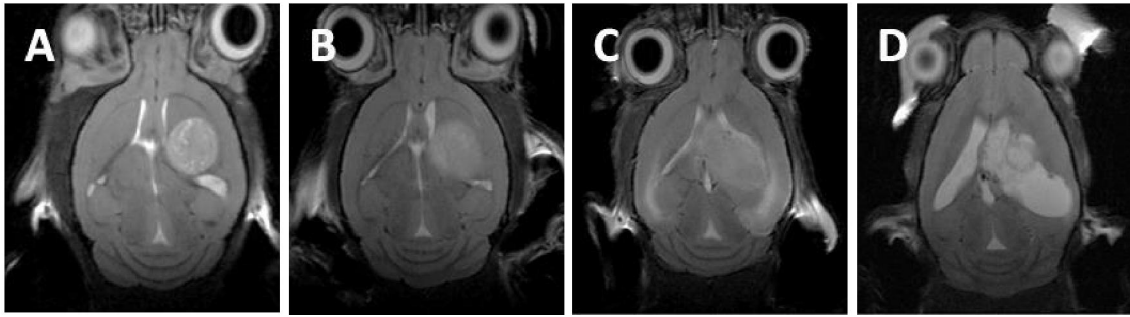


Fig. 1 Coronal T_{2w} MRI of mice brains with different appearance of tumours, depending on type of cells implanted **A)** tumour C482 generated with standard GL261 cells (from the repository of C57BL/6 mice with GL261 GBM explored in the group in the period 2010-2011), 15 days post tumour detection **B)** tumour G10-S912 from ‘short latency’ group generated from fresh CDT, 19 days post tumour detection **C)** tumour Gc5-S912 from ‘short latency’ group generated from frozen S912 CDT, 20 days post tumour detection **D)** ventricular obliterating tumour Gc8-S912 from ‘intermediate latency’ group generated with frozen S912 CDT, 46 days post tumour detection

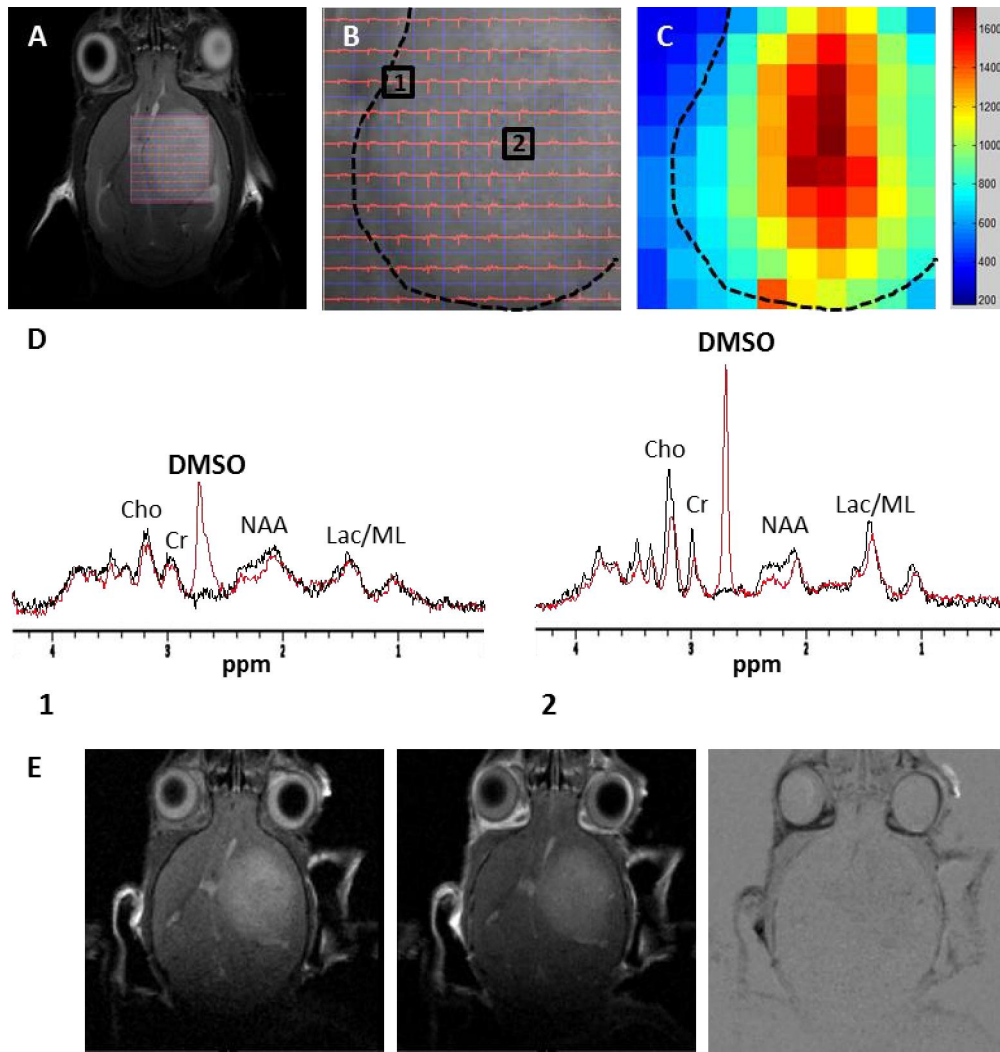


Fig. 2 Representative DMSO-MRSI of the animal G6-S912 acquired at TE 14ms at 34 days p.i.: **A)** VOI superimposed with the reference image (T_{2W} MRI). **B)** Enlargement of VOI: black dotted line labels the tumoural mass and black squares 1 and 2 correspond to the voxels of the matrix from which SV spectra were extracted and shown in D). **C)** Color-coded intensity map representing the relative DMSO signal (as described in [21]) detected at 66 minutes after its i.p. administration. **D)** Spectra of voxels marked as 1 (low accumulation zone) and 2 (high accumulation zone) in the MRSI grid shown in B before (black spectrum) and 66 minutes after the administration of DMSO (red spectrum). Cho: choline containing compounds, Cr: total creatine, NAA: N-acetylaspartate, Lac/ML: Lactate/mobile lipids. **E)** Coronal T_{1W} MRI pre- (left) and post- (middle) contrast administration and subtraction of the two previous images (right) of the animal G6-S912 acquired 34 days p.i.

1
2
3
4
5
6
7
8
9
10
11
12
13
14
15
16
17
18
19
20
21
22
23
24
25
26
27
28
29
30
31
32
33
34
35
36
37
38
39
40
41
42
43
44
45
46
47
48
49
50
51
52
53
54
55
56
57
58
59
60
61
62
63
64
65

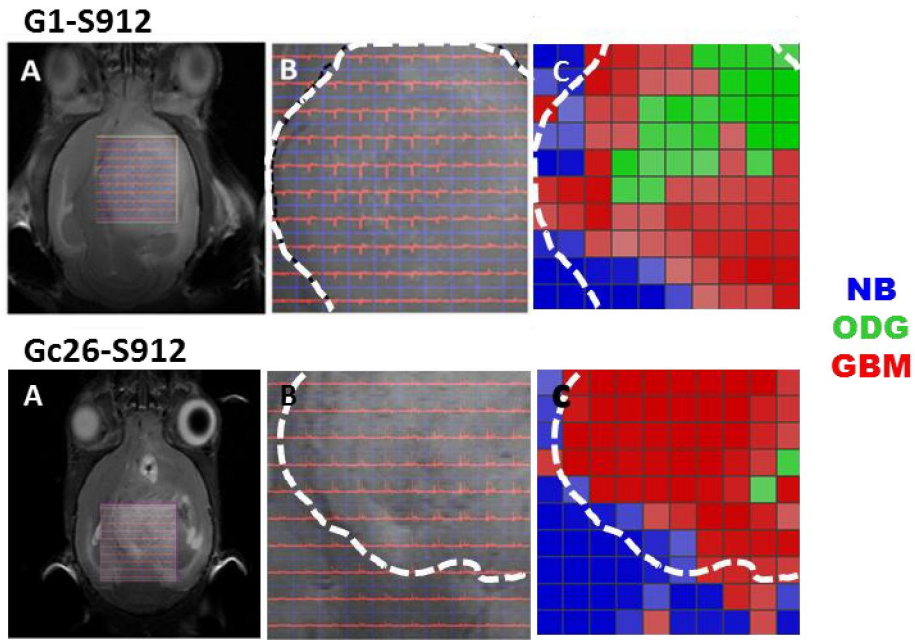


Fig. 3 Pattern recognition analysis for two representative animals from groups D and E of Supplementary Table 1, implanted with fresh CDT, G1-S912 (top) at day 39 p.i. and frozen CDT, Gc26-S912 (bottom) at day 35 p.i. **A)** VOI superimposed with the reference image (T_{2w} MRI). **B)** Enlargement of VOI shown in A with spv for short TE in red. **C)** Nosological maps. Blue voxels are assigned to normal brain parenchyma (NB), red voxels to GBM and green voxels to ODG. Tumour boundaries from T_{2w} images are marked with a white dotted line

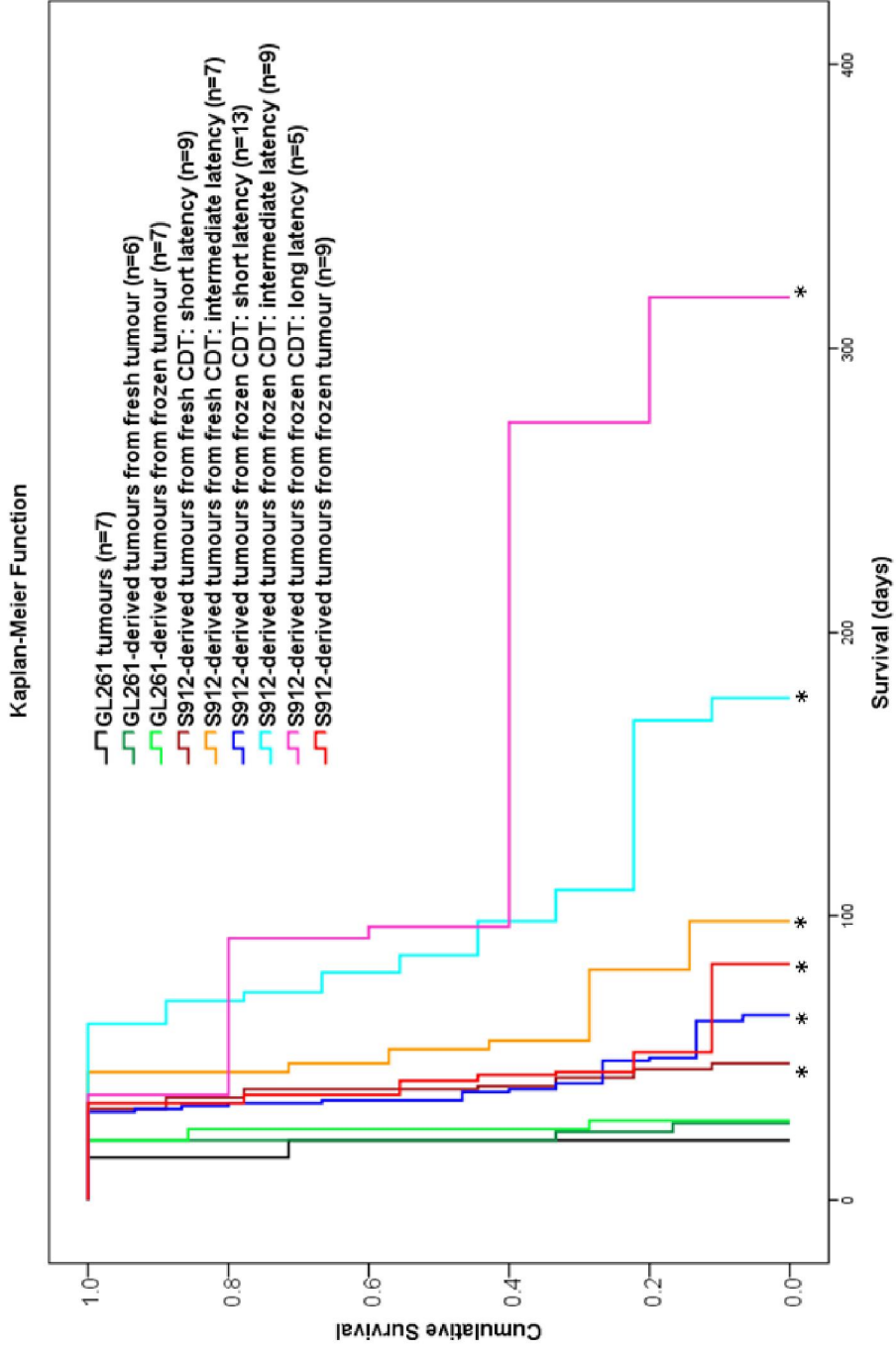
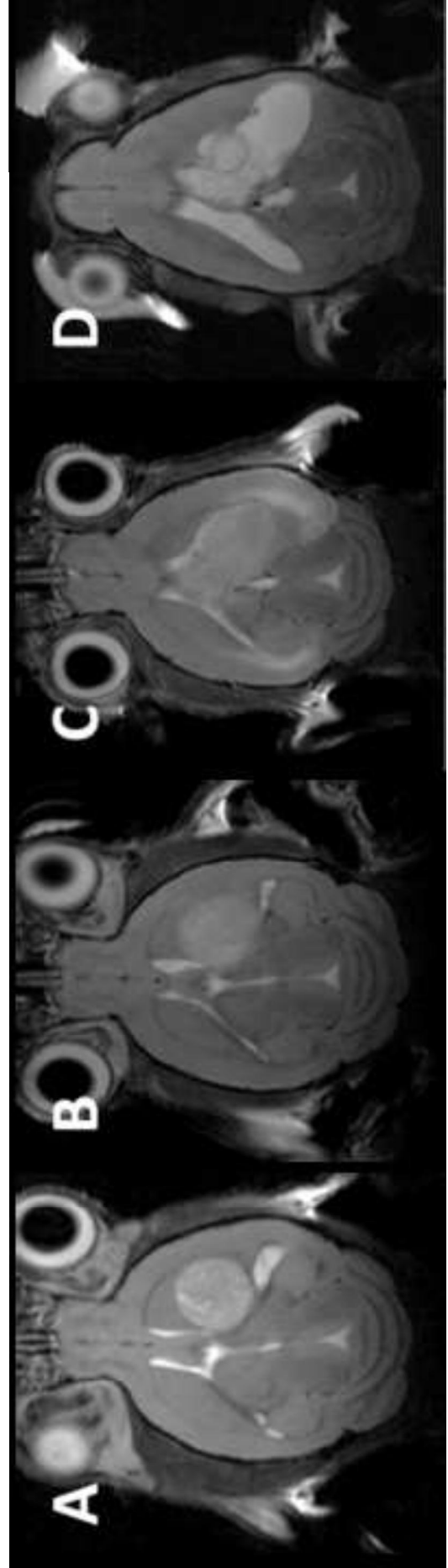
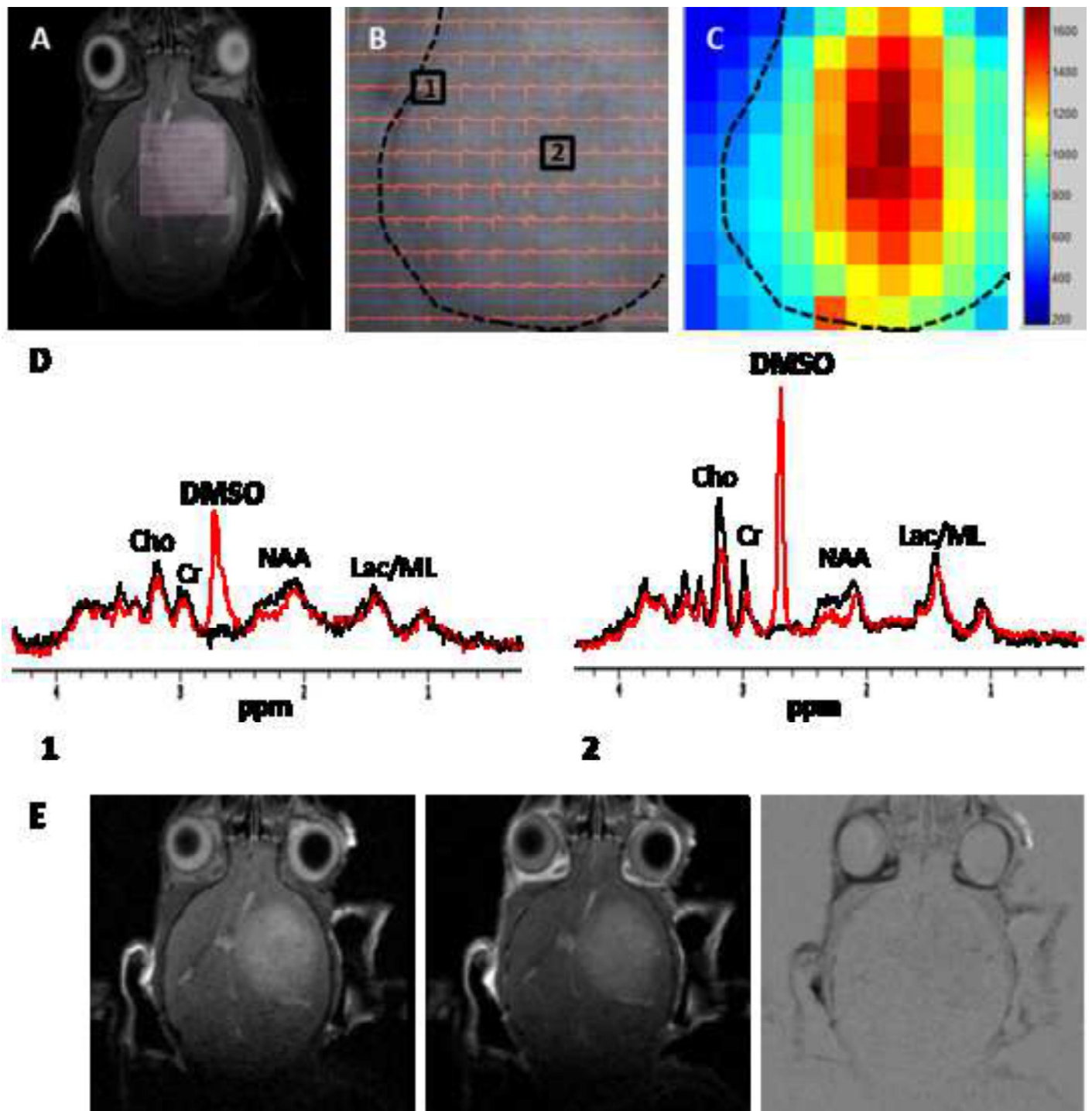
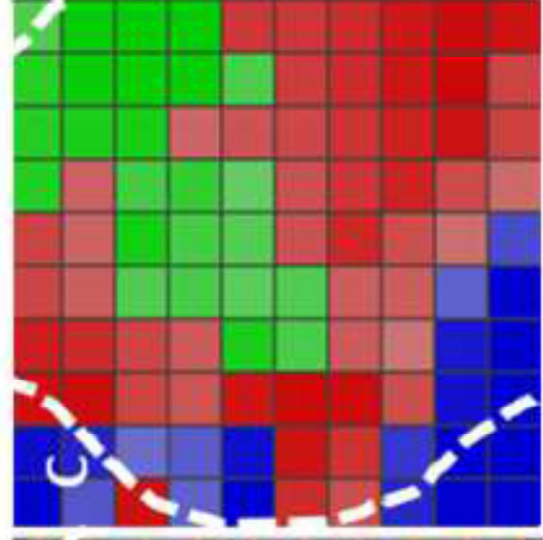
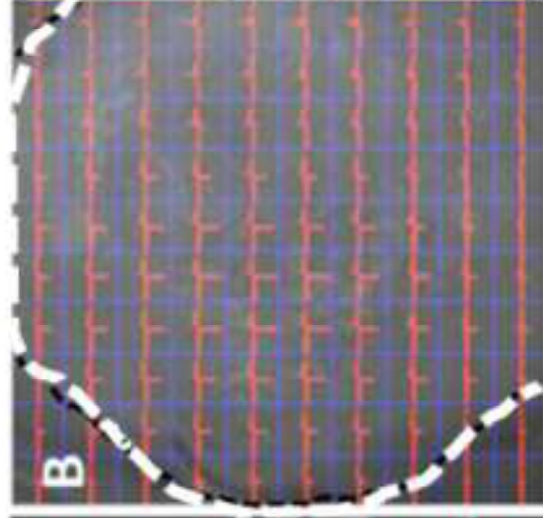
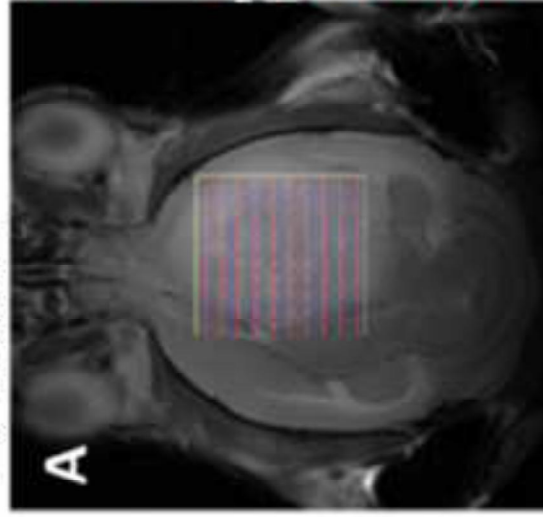


Fig. 4 Kaplan-Meier survival curves of C57BL/6 mice implanted with cells of different origin or different preparation protocol. Survival of the animals implanted with cells from S912 CDT was significantly higher (marked with asterisk) in comparison with those implanted with GL261 cells or GL261 CDT. See Supplementary Table 2 for further details

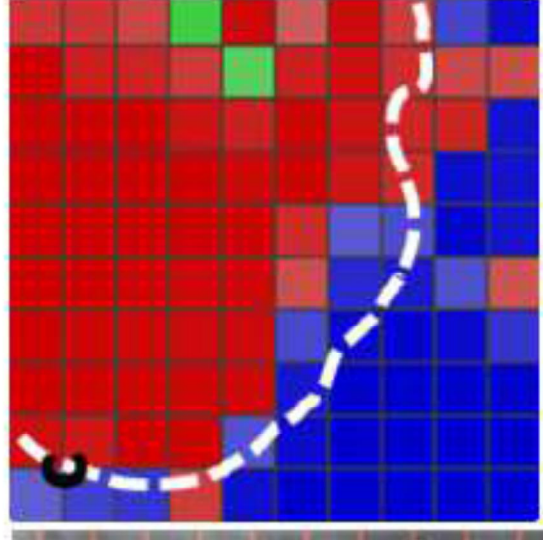
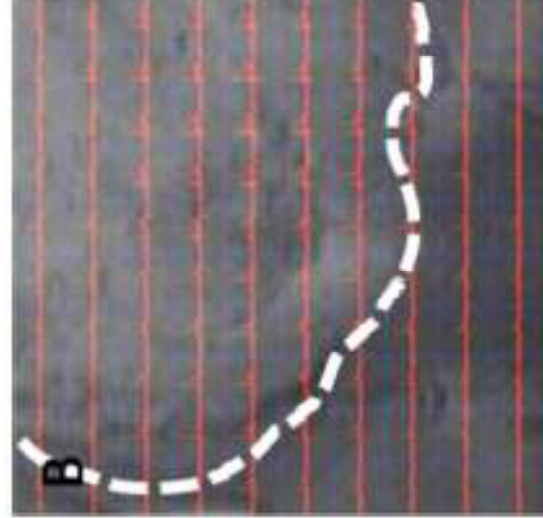
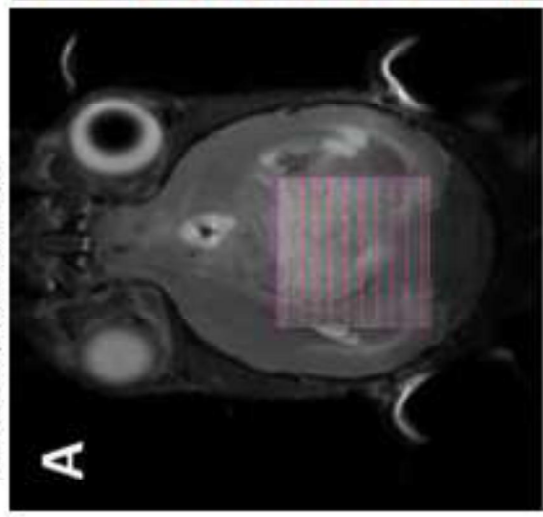




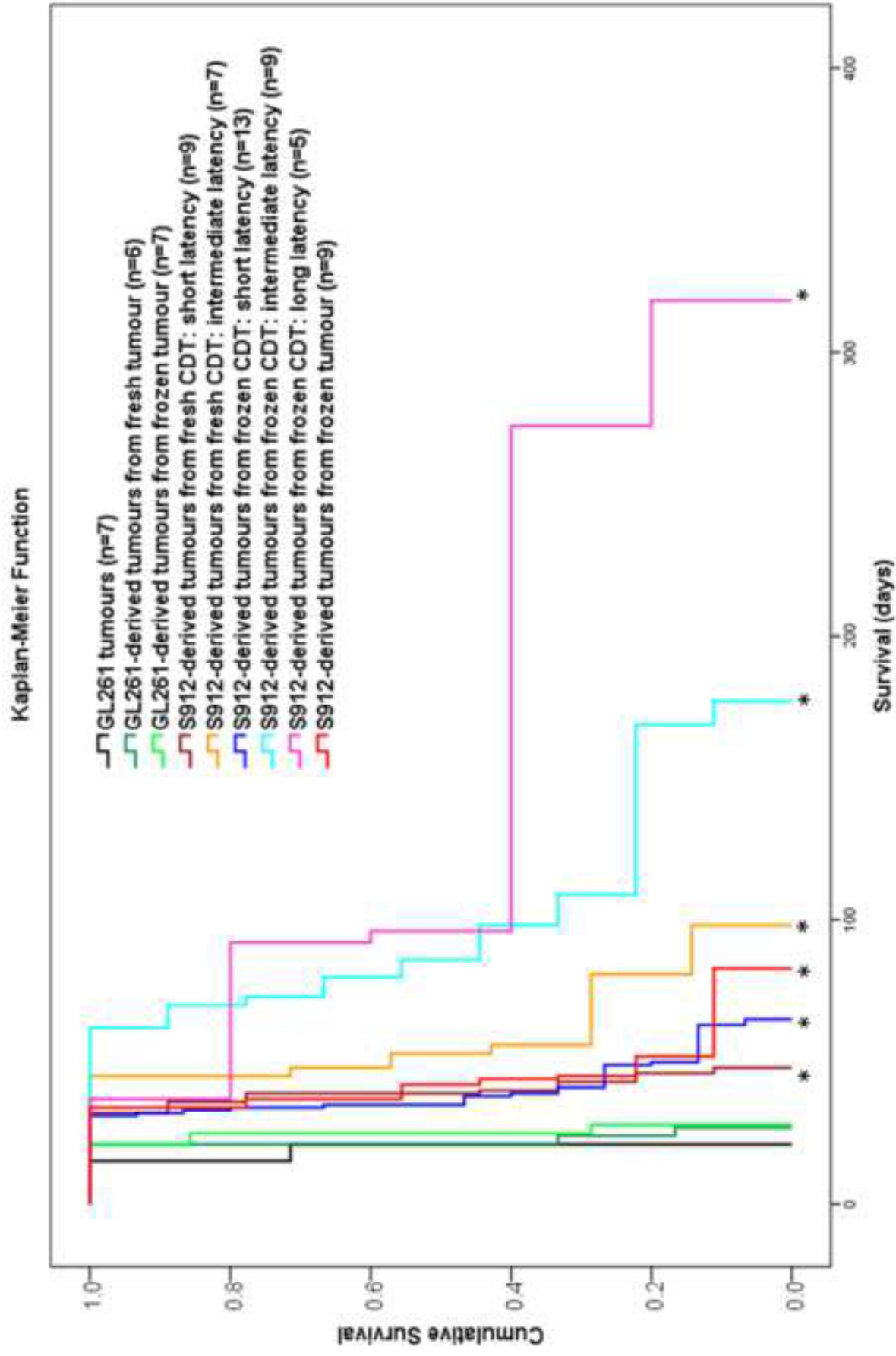
G1-S912

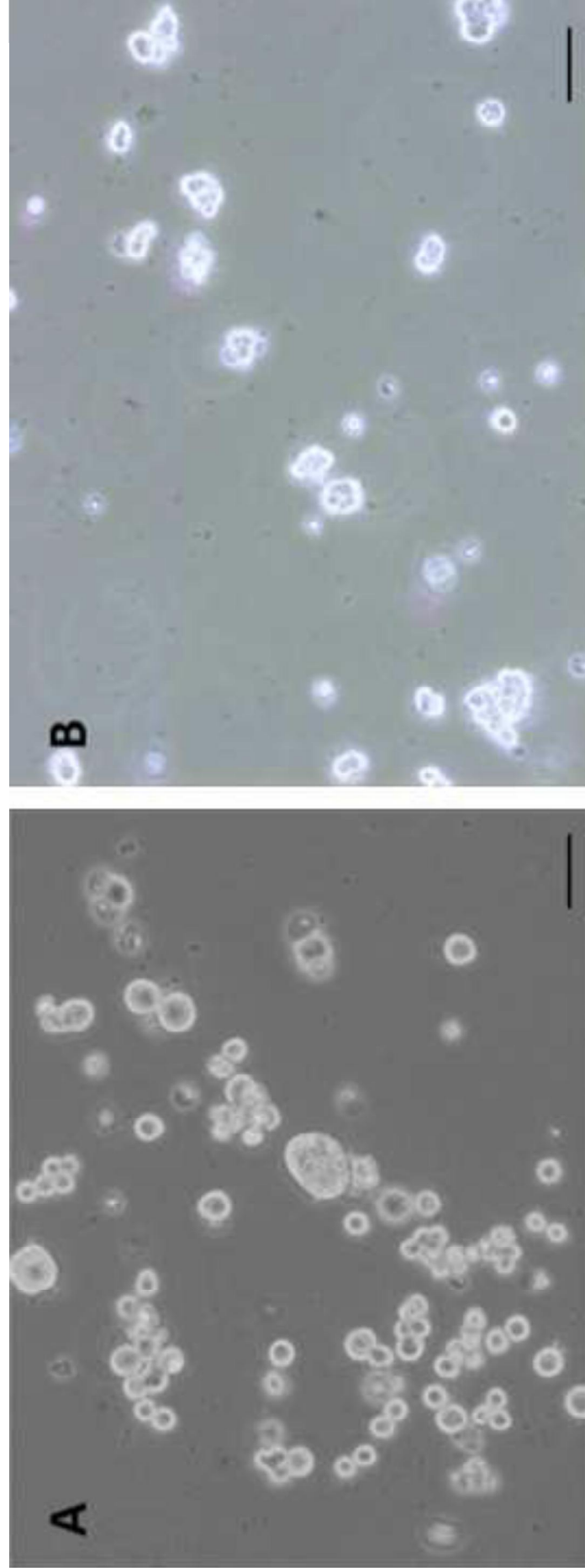


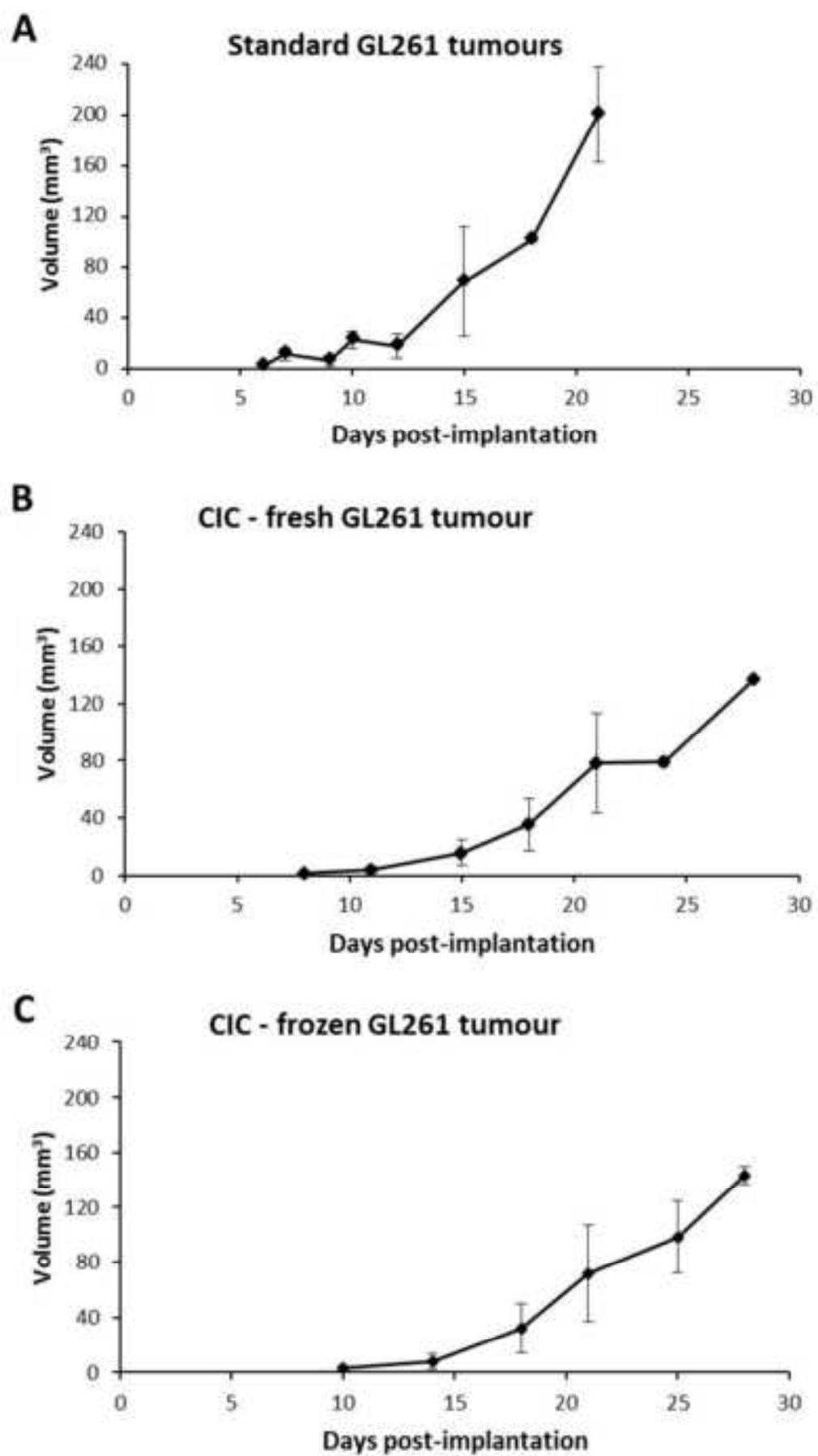
Gc26-S912

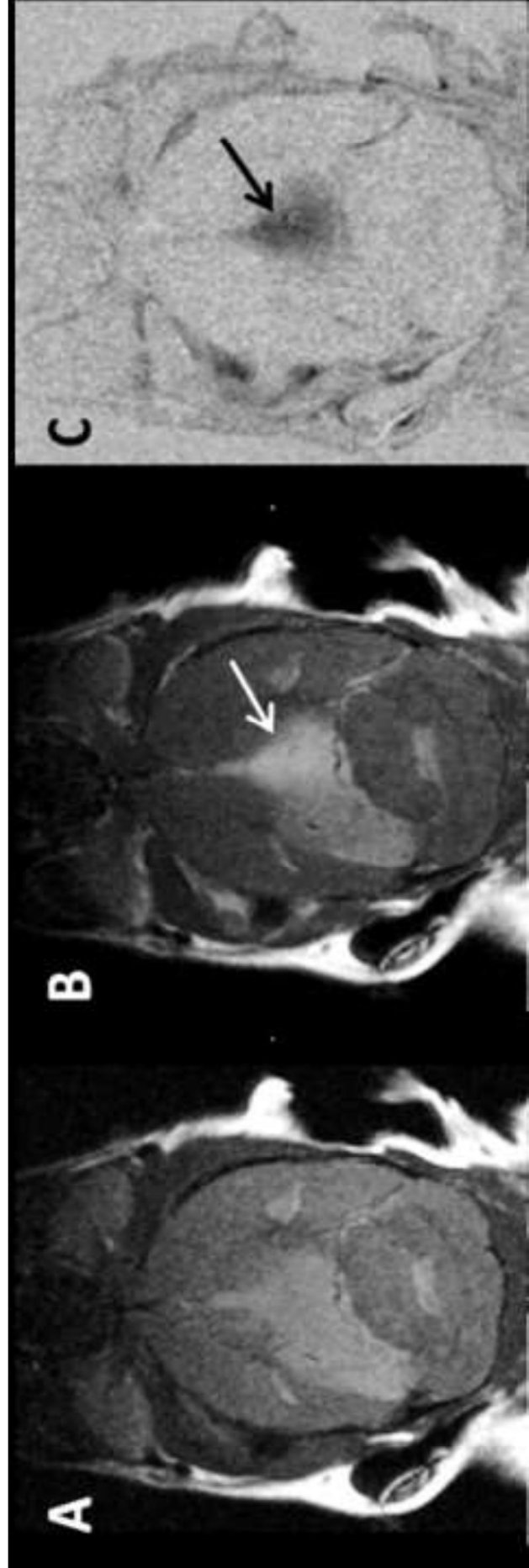


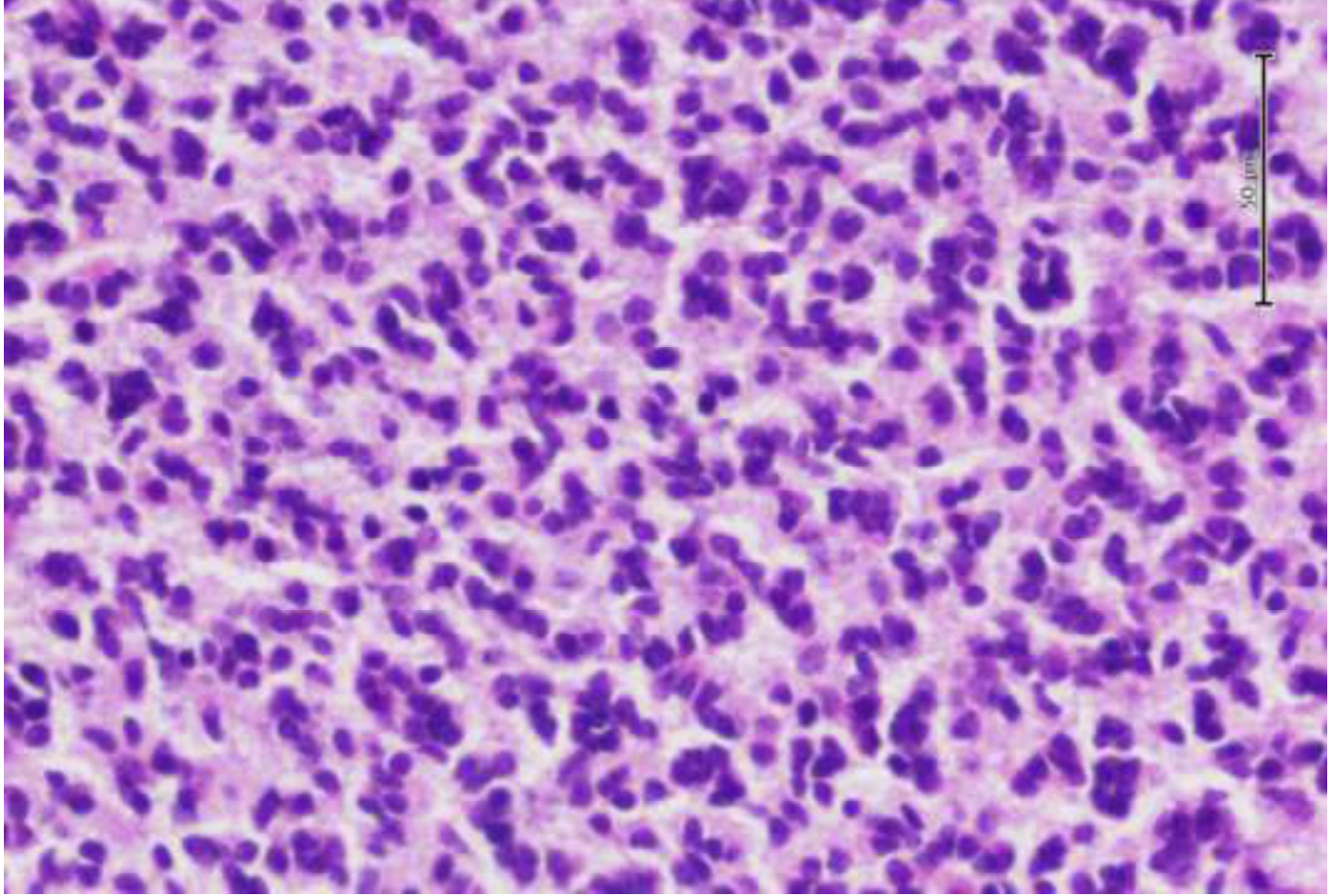
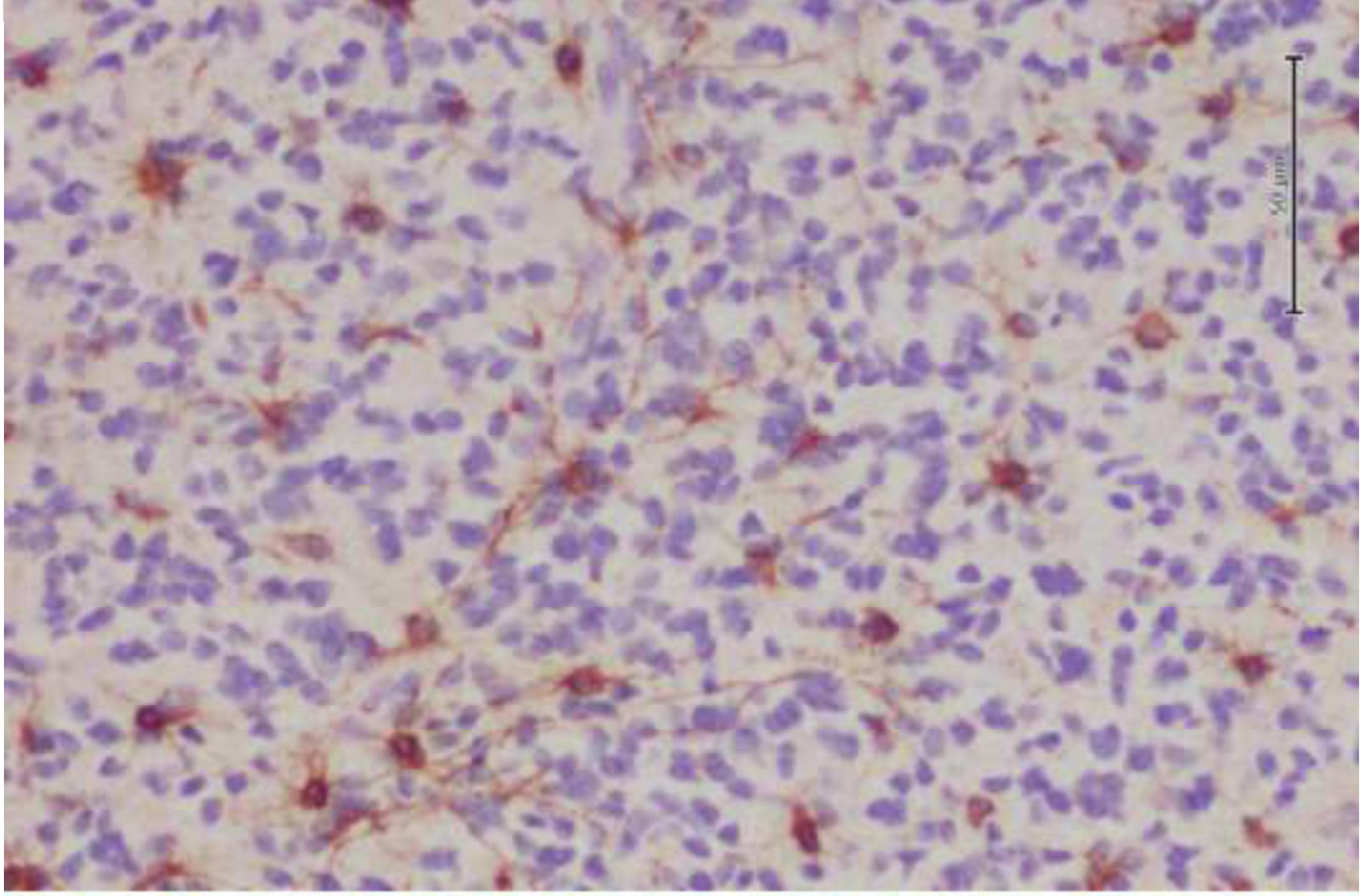
NB
ODG
GBM

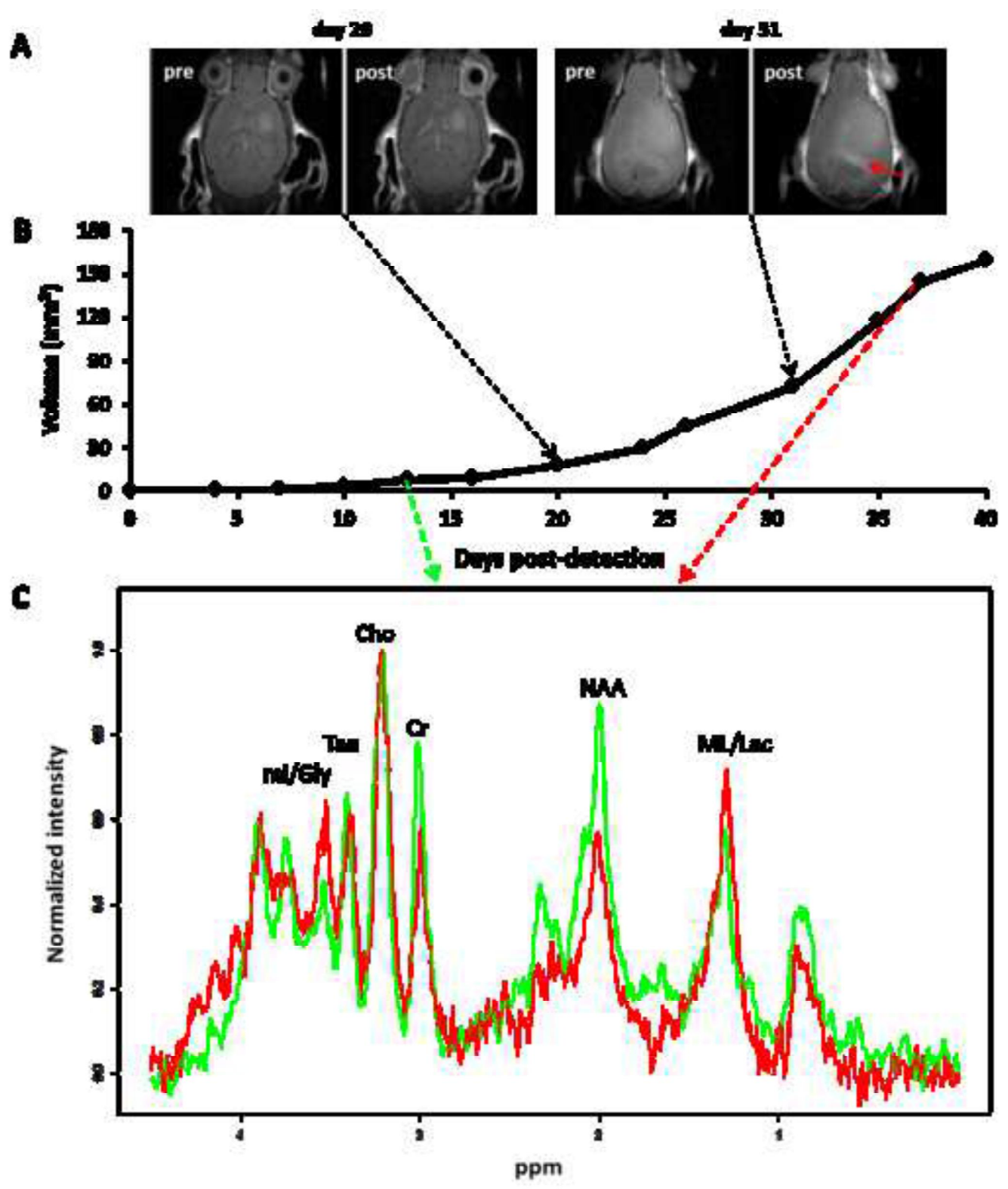


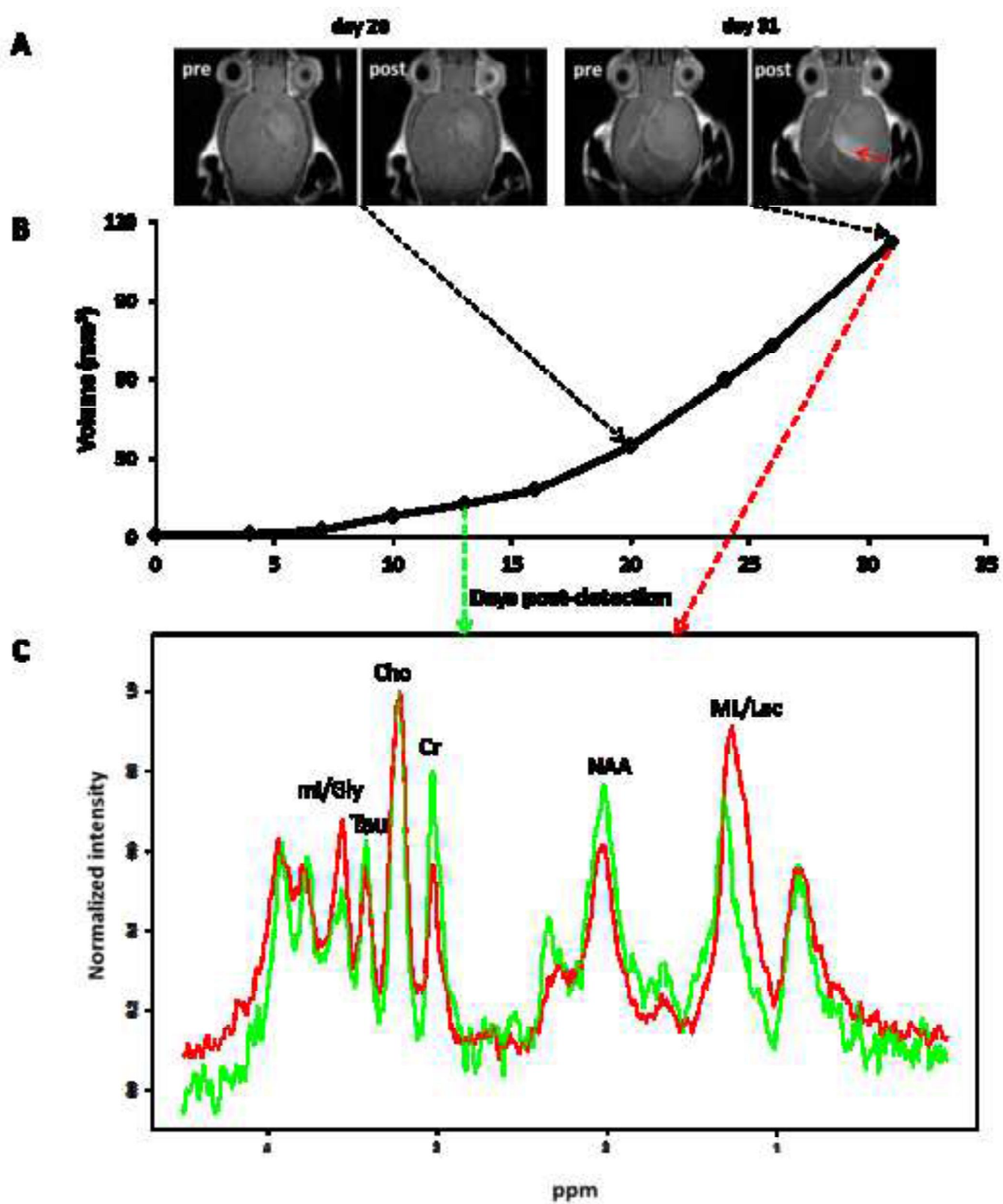


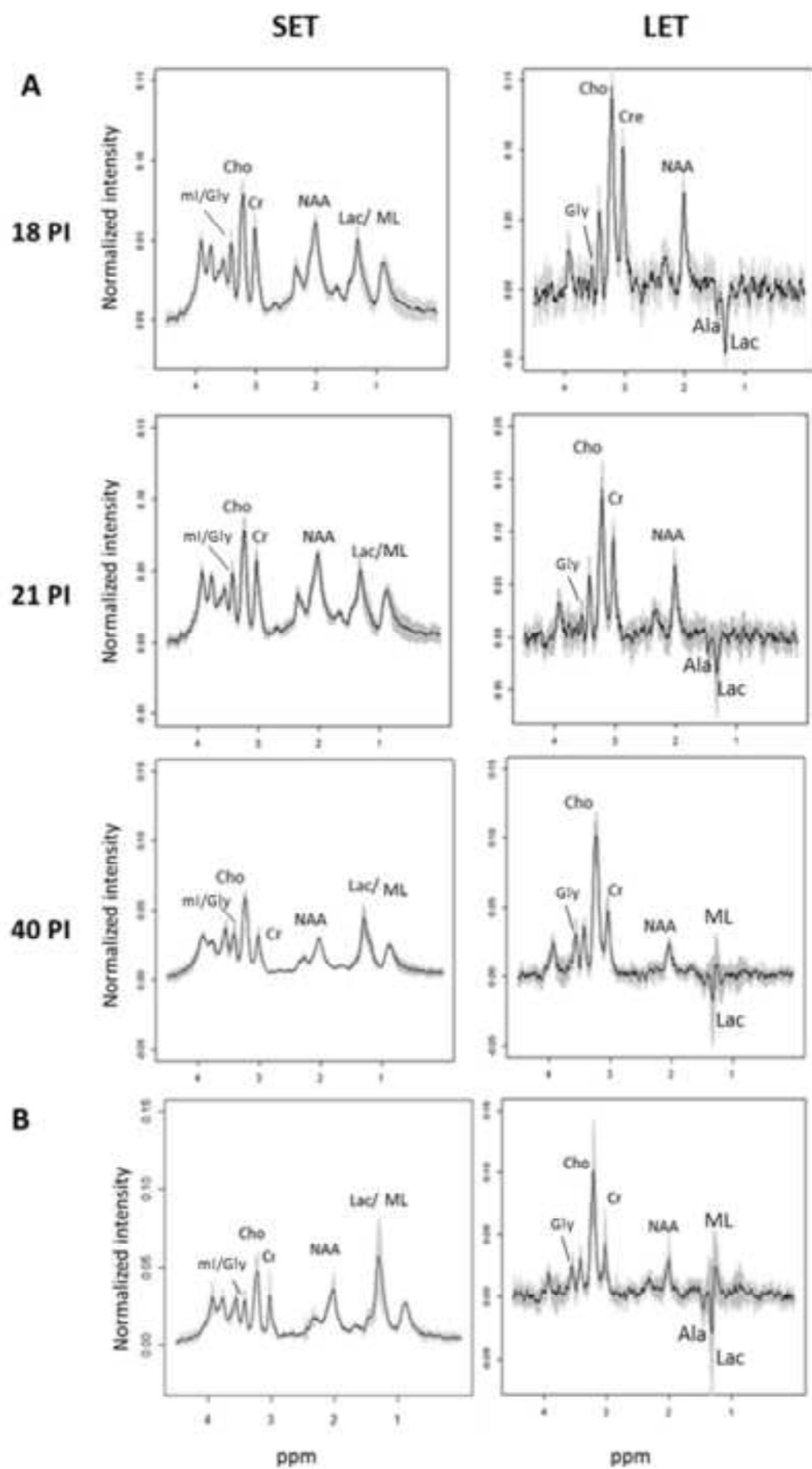


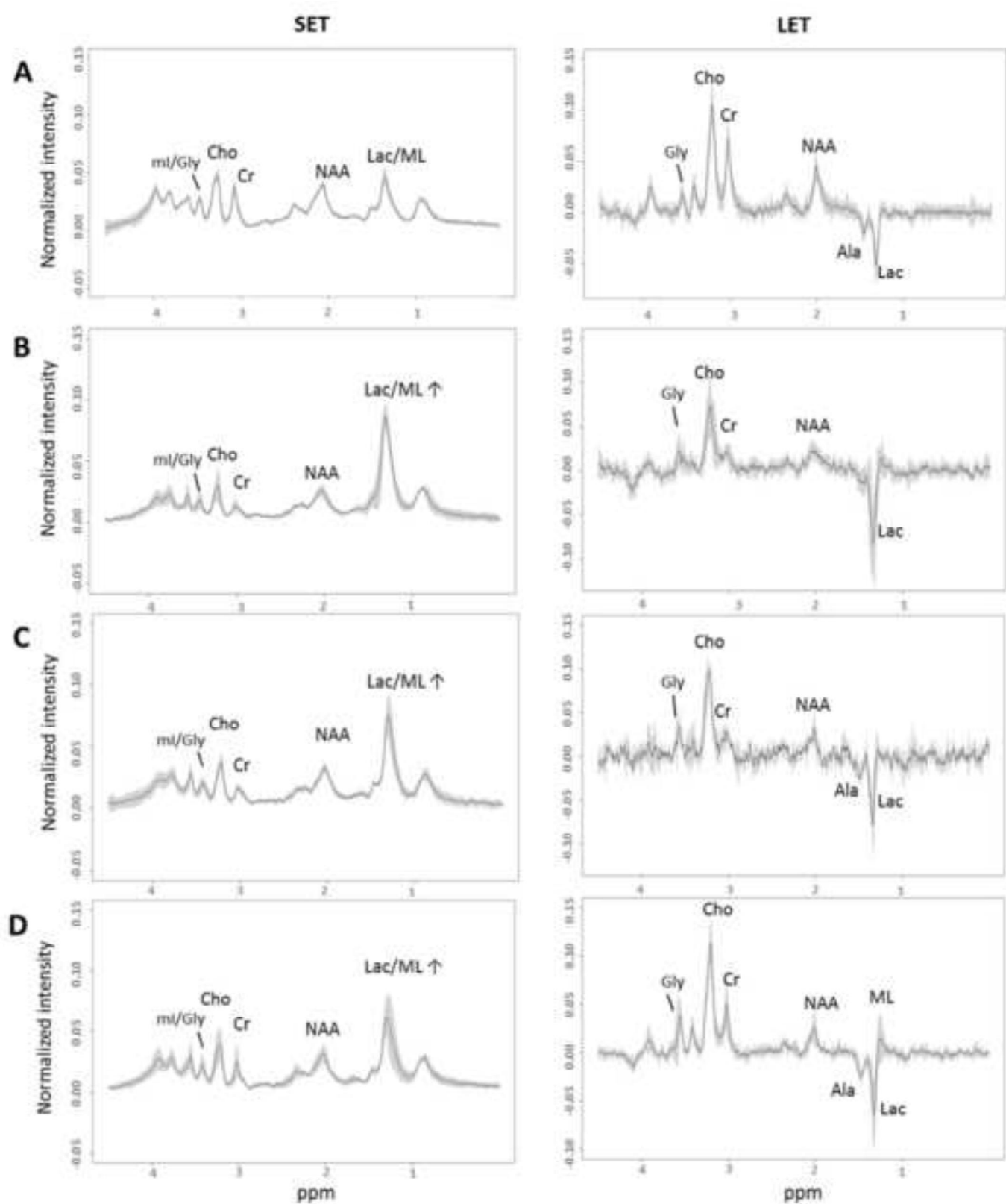


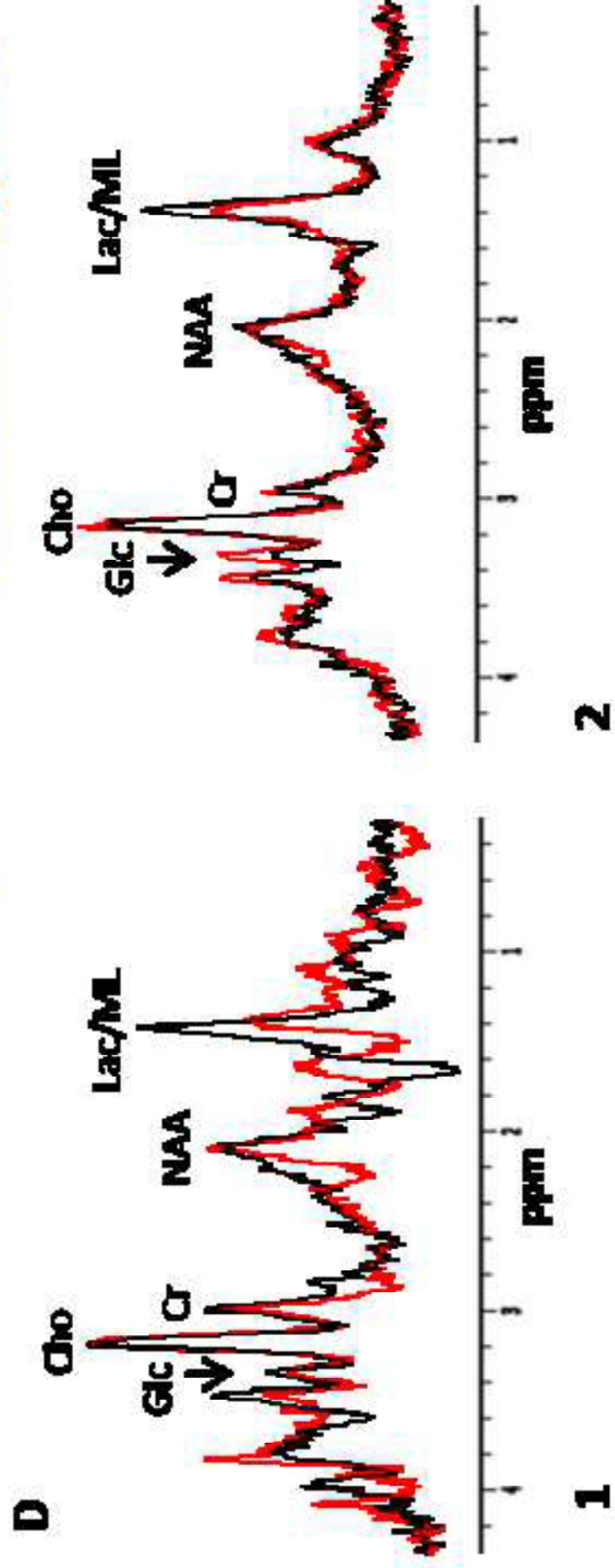
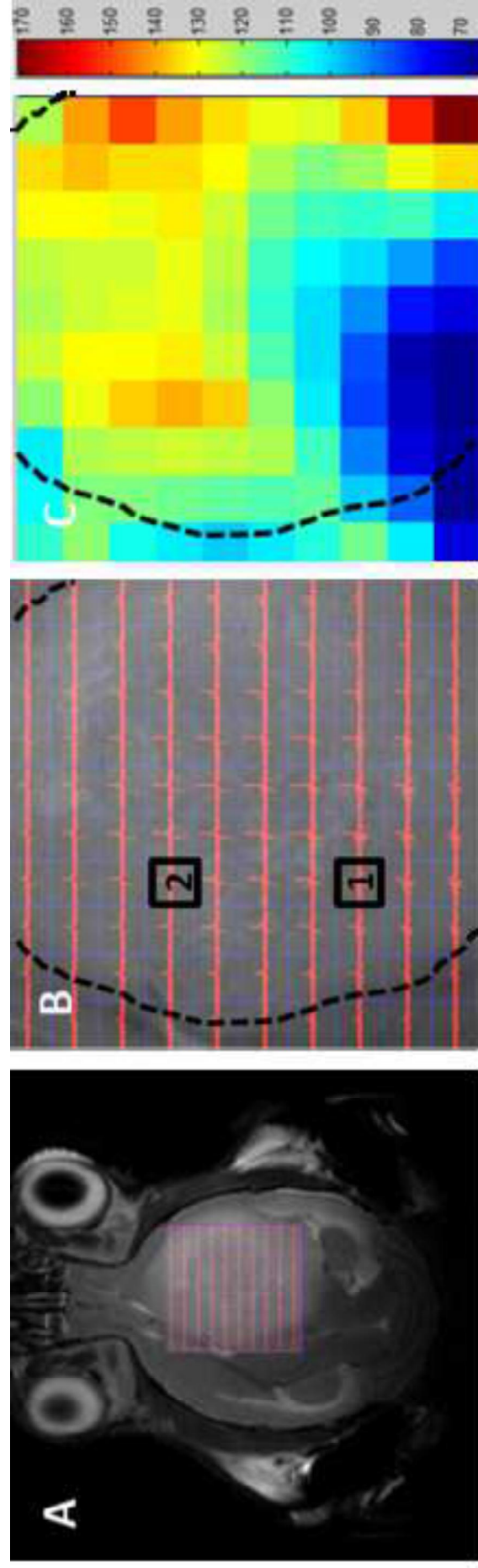












SUPPLEMENTARY MATERIAL FOR:
DEVELOPMENT OF A TRANSPLANTABLE GLIOMA TUMOUR MODEL
FROM GENETICALLY ENGINEERED MICE. MRI/MRS/MRSI
CHARACTERISATION

Magdalena Ciezka, Milena Acosta, Cristina Herranz, Josep M. Canals, Martí Pumarola, Ana Paula
Candiota, Carles Arús.

SUPPLEMENTARY METHODS

CDT Culture

CDT cultures were obtained by seeding Corning 75 cm² flasks (Sigma-Aldrich Co.) with 10,000 cells/cm² in Complete Medium [Dulbecco's Modified Eagle's Medium (DMEM; Sigma-Aldrich Co.):F12 (GIBCO) (1:1); supplemented with 30% D-(+)-glucose, 0.2 % heparin, 4 mg/ml bovine serum albumin, 10 ng/ml fibroblast growth factor (all from Sigma-Aldrich Co.), 0.3 mg/ml glutamine, 50 U/ml penicillin/streptomycin, 5 mM HEPES, 1× N2 supplement (all from GIBCO) and 20 ng/ml epidermal growth factor (Invitrogen SA)]. Cell cultures were incubated at 37°C in a 5% CO₂ atmosphere.

Every 5 days, CDT aggregates were collected, centrifuged at 1000 g during 7 minutes and dissociated by pipetting approximately 40 times with a 100 µl of medium using a P100 micropipette and re-plated in fresh medium at a density of 10,000 cells/cm² in multi-well plates. All cell cultures were incubated at 37°C in a 5% CO₂ atmosphere.

Some CDT aggregates were frozen to check the reliability, robustness and repeatability of generated cells for transplantation purposes. For this, two days after disaggregation and cultivation, CDT were centrifuged and transferred to the freezing medium: 90% Complete Medium with 10% DMSO (Sigma-Aldrich Co.). The cells (range 30,000 – 100,000) were loaded into a cryovial and frozen (at the rate of -1°C/min until -80°C) using a freezing container (Nalgene Europe Ltd., Hereford, UK), and then stored in liquid nitrogen. When needed for further use, CDT aggregates were rapidly thawed in a water bath at 37°C, washed twice in DMEM and cells from CDT dissociated and cultured as described above.

In vivo MRI/MRS/MRSI

MR studies were carried out at the Unit 25 of NANBIOSIS, a joint NMR facility of the Universitat Autònoma de Barcelona and CIBER-BBN (Cerdanyola del Vallès, Spain) with a 7T horizontal magnet (BioSpec 70/30, Bruker BioSpin, Ettlingen, Germany) equipped with actively shielded gradients (B-GA12 gradient coil inserted into a B-GA20S gradient system) and a quadrature receive surface coil, actively decoupled from a volume resonator with 72 mm inner diameter.

Mice were placed in the scanner bed and anesthetized with 0.5-2.0% isoflurane in O₂, keeping the respiratory frequency at 60-80 breaths/min. The body temperature was controlled using a recirculating water system incorporated to the animal bed, measured by a rectal probe and maintained between 37-38°C, except in the case of PE-MRSI glucose studies, when the temperature was maintained between 28.5 - 29°C. Breathing and temperature were constantly monitored (SA Instruments, Inc., New York, USA).

MRI acquisition

GEM bearing S100 β -v-erbB / inK4a-Arf (+/-) transgene/KO, as well as GL261 tumour-bearing mice were screened by acquiring high resolution coronal T_{2w} images (TR/TE_{eff} = 4200/36 ms) using RARE (Rapid Acquisition with Relaxation Enhancement) sequence to detect brain tumour presence and monitor its evolution stage. The acquisition parameters were as follows: turbo factor, 8; field of view (FOV), 19.2 x 19.2 mm; matrix, 256 x 256 (75 x 75 μ m/pixel); number of slices, 10; slice thickness (ST), 0.5 mm; inter-ST, 0.6 mm; number of averages (NA), 4; total acquisition time (TAT), 6 min and 43 s.

SV-MRS acquisition

Once tumours reached a volume sufficient for setting a voxel of the size (2 - 3 mm)³ without contaminating the metabolic profile with normal brain parenchyma, SV spectra were acquired at short and long echo time (TE), 12 and 136 ms respectively, using PRESS localization and VAPOR water suppression [1], and using the parameters described in [2]: spectral width (SW), 4006.41 Hz; TR, 2500 ms; NA, 128; TAT, 5 min and 30 s.

Contrast Enhanced MRI (CE MRI)

Animals were studied by CE MRI to evaluate BBB integrity by acquiring standard T_{1w} images (TR/TE=350/8.5ms) before and 20 minutes after intraperitoneal (ip) injection of gadoterate meglumine (DOTAREM, Guerbet, Roissy, France) as a bolus (200 μ l, 50 μ mol/ml in saline).

MRSI and PE-MRSI

A total of thirty-seven tumour-bearing mice were studied by PE-MRSI with DMSO administration [2] and/or (according to the BioSpec scanner availability) by PE-MRSI with glucose in

hypothermia [3]. Supplementary Table 3 states the number of animals and explorations carried out for each condition. Both substances used in PE-MRSI studies were injected ip as a bolus (10 µl per g of animal, 10% (v/v) DMSO and 25% (w/v) D-glucose in saline, respectively), while the animals were inside the magnet, to avoid re-shimming needs.

For the PE-MRSI with DMSO, a coronal T_{2w} high resolution reference image and 14 ms TE basal MRSI were initially acquired. DMSO was then injected, followed by three repeated 14 ms TE MRSI acquisitions. For the PE-MRSI with glucose in hypothermia studies, a coronal T_{2w} high resolution reference image and two reference scans were initially acquired, one with 14 ms TE, followed by 136 ms TE. Then, hyperglycemia was induced and consecutive MRSI scans were acquired as follows: 14 ms TE, 14 ms TE, 14 ms TE, 136 ms TE and 14 ms TE.

Experiments were performed using a 2D CSI (Chemical Shift Imaging) sequence with PRESS localization, where: FOV, 17.6 x 17.6 mm; ST, 1 mm; Volume of Interest (VOI), 5.5 x 5.5 x 1.0 mm, positioned in the way that most tumour was covered, and including a part of the nearby normal/peritumoural brain parenchyma; TR, 2500ms; SW, 4006.41Hz; NA, 512; TAT, 21m 30 s.

Water suppression was performed with VAPOR, using a 300 Hz bandwidth. Linear and second order shims were automatically adjusted with FASTMAP in a 5.8 x 5.8 x 5.8 mm volume which contained the VOI region. Six saturation slices (ST, 10 mm; sech-shaped pulses: 1.0 ms/20250 Hz) were positioned around the VOI to minimize outer volume contamination in the signals obtained. Spatial resolution was defined by a 8 x 8 voxel matrix over the FOV (4.84 µl nominal resolution) reconstructed after Fourier interpolation to a 32 x 32 matrix, as described in [3].

MR data post-processing

Tumour volume calculation

Tumour volumes for mice in groups of interest were calculated from T_{2w} high resolution horizontal images using equation (1):

$$TV(mm)^3 = [(AS_1 + ST) + [(AS_2 + (...)) + AS_{10}) \times (ST + IT)]] \times 0.075^2 \quad \text{Eq. (1),}$$

where TV is the tumour volume, AS_x is the number of pixels contained in the region of interest delimited by the tumour boundaries in each slice of the MRI sequence, ST is the slice thickness (0.5 mm), IT is the inter-slice thickness (0.1 mm) and 0.075^2 is the individual pixel surface area (mm^2).

The tumour area was calculated in pixels in each slice, using the Paravision 5.0 software (Bruker BioSpin, Ettlingen, Germany) and an automated system for generating regions of interest (ROIs).

Calculation of tumour doubling time

Doubling time (DT) of abnormal masses was calculated using equation (2) as in [4]:

$$DT = \frac{(T-T_0) \times \ln 2}{\ln(V/V_0)} \quad \text{Eq. (2),}$$

where $T-T_0$ indicates the length of time between two measurements and V_0 and V denote the tumour volume at two points of measurement, the initial and the final, respectively.

MRS post-processing

In vivo MR SV spectra were processed with the TopSpin v1.3 software (Bruker Daltonik, GmbH): Lorentzian filter, 4 Hz of line broadening before Fourier transformation, manual zero- and first-order phase correction were applied and chemical shift was referenced to total creatine (3.03 ppm). The spectra were exported in ASCII format and analysed with the software R v2.15.2 (The R Foundation for Statistical Computing) using home-written scripts for UL2 normalization [5] (as per equation 3) and average spectra and SD calculation. Spectral metabolite heights for major resonances were calculated from 0.5 to 4.5 ppm for each spectrum.

$$I_{norm}i = \frac{I_{real}i}{\sqrt{\sum_0^{4.5} (I_{real}i)^2}} \quad \text{Eq. (3),}$$

where $I_{norm}i$ is the normalized intensity for each point of the spectrum and $I_{real}i$ is the initial intensity for each point between 0 and 4.5 ppm

MRSI post-processing

MRSI data were post-processed essentially as described in reference [3]. Briefly, data were initially pre-processed at the MR workstation with ParaVision 5.0 (Bruker BioSpin), and then post-processed with 3D Interactive Chemical Shift Imaging (3DiCSI) software package (courtesy of Truman Brown, Ph.D., Columbia University, New York, NY, USA) for line broadening adjustment (Lorentzian filter, 4 Hz), zero-order phase correction and exporting the data in ASCII format.

Dynamic MRSI processing Module (DMPM) [6] running over MatLab (The MathWorks Inc., Natick, MA, USA) was used to align all spectra within each MRSI matrix (using the choline containing compounds peak as reference, 3.21 ppm), quantify the relative peak intensity changes (2.72 ppm for DMSO and 3.43 ppm for glucose) and display these changes as color-coded maps (10 x 10 voxels). The 0 – 4.5 ppm region of each spectrum in the MRSI matrix was individually normalized to UL2 and the normalized matrix was exported in ASCII format for performing the pattern recognition (PR) analysis.

Pattern recognition

The pattern recognition analysis was used to classify which voxels from the glucose-perturbed MRSI matrices corresponded to normal brain tissue, ODG or GBM, and it was carried out using *SpectraClassifier* software [7] (available at <http://gabrmn.uab.es/sc>) and a previously developed classifier, as described elsewhere [8]. Each individual voxel in the MRSI grid was referred to as spectral vector (spv) and considered as an individual case. The result obtained was represented as colour-coded nosological maps for each matrix.

Tissue preservation for post-mortem procedures

In vivo MR studies and follow up of the tumour progression took place until animals died or were sacrificed, due to animal welfare standard protocol, by cervical dislocation. The brains of 49 mice in total (S912 and its derivatives) were excised and fixed in 4% formaldehyde and embedded in paraffin. Transversal sections 5 µm thick were cut and analysed by classical Hematoxylin-Eosin staining, as well as by immunohistochemistry analysis for oligodendrocyte transcription factor (Olig2) protein as oligodendroglial marker and glial fibrillary acid protein (GFAP) as astroglial marker. Classification and grading of tumours were performed according to the criteria defined by the World Health Organization (WHO) human classification for central nervous system tumours [9].

In case of S912-derived tumours with an apparent low/intermediate grade by MRI/MRSI, see results, (i.e. no BBB breakdown; MRS SV pattern) (n=5), these were extracted and halved – one part was used for histopathological analysis, while another part was frozen in liquid nitrogen in cryotubes containing 1ml of 10% DMSO in Phosphate Buffered Saline (PBS) for future disaggregation and potentially obtaining second generation of CDT culture. Tumours from randomly chosen animals (n=7) were also used to perform genotype check.

Genotype check

Transgene presence and knock-out mutations in the GEM S912 mouse were confirmed by PCR (polymerase chain reaction) analysis according to slight modifications of the protocols kindly provided by Dr David Goldberg (University of California San Francisco, USA) and Dr Dave Sims (MMHCC-NCI, USA). Briefly, DNA was extracted overnight at 55°C from a tail fragment of the mouse with a standard lysis solution: 50 mM Tris-HCl pH = 8, 1 mM EDTA, 0.2% SDS, 20 mM NaCl, 100 mg l⁻¹ proteinase K. For S100b-v-ErbB amplification, primers (all obtained from Thermo Fisher Scientific GmbH, Ulm, Germany) 5'-CTCACAGCAATCTCAAAGCTCCCC-3' and 5'-AGCCTCAAAGTCAGGTTGATGAGC-3' were used, as described in [10]. For Ink4a-Arf (+/-) three

other primers were used instead: 5'-GTGATCCCTCTACTTTTTCTTCTGACTT-3', 5'-CGGAACGCAAATATCGCAC-3', and 5'-GAGACTAGTGAGACGTGCTACTTCCA-3'. Cycling conditions were as follows: one cycle of 95°C for 5 min followed by 29 cycles at 95°C for 1 min, 60°C for 30 s, 72°C for 2 min and finished with one cycle at 72°C for 10 min. Selected S912-derived tumours were checked for the presence of the transgene and knock-out mutations by the same extraction and PCR procedure, performed on a piece of tumour, to confirm the accordance of the genotype with the original S912 GEM. A total of 9 animals were analysed: 4 animals implanted with CDT cultured from freshly disaggregated S912 tumour, 3 animals implanted with previously frozen S912 CDT and 2 animals implanted with CDT cultured from a frozen piece of S912 tumour.

Statistical analysis

The statistical analysis was carried out using IBM SPSS Statistics v.20 software. The survival rate of treated and untreated mice was calculated using Kaplan-Meier analysis. Metabolite height ratios from SV MRS spectra were inspected for normality with the Kolmogorov-Smirnov test, compared using the Student's t-test for paired samples and the Mann-Whitney U-test was applied to non-normal distributions, while variance homogeneity was studied with the Levene's test. Significance level was set to 0.05.

SUPPLEMENTARY RESULTS

Passage of tumours obtained from disaggregation of GL261 GBM

GL261 tumour bearing mice were sacrificed once masses reached a volume of $140 \pm 20 \text{ mm}^3$ (n=6, day 18 ± 2 p.i.) and tumour tissue was used to generate CDT cultures (Supplementary Figure 1A).

CDT obtained from fresh GL261 GBM

Tumours were detectable by MRI on the day 8 p.i. in all implanted mice and had a mean survival of 21 ± 3 days (Supplementary Figure 2). The final mean volume of those tumours was $101 \pm 26 \text{ mm}^3$, significantly smaller (p=0.049) in comparison to $169 \pm 59 \text{ mm}^3$ in control GL261 tumours from our group [11]. The penetrance obtained was 100%.

CDT obtained from frozen GL261 GBM

Abnormal masses were detectable by MRI on the day 10 p.i., resulting in a slightly longer (although not significant, p=0.106) survival (25 ± 2 days) in comparison with the group implanted with freshly disaggregated tumours (Figure 4, Supplementary Figure 2 and Supplementary Table 2). The

penetrance was 100% and the mean final tumour volume was of $119\pm 32\text{ mm}^3$, non-significantly different from control GL261 ($p=0.078$) and tumours generated with fresh CDT from GL261 tumour ($p=0.295$).

CE-MRI studies

Regarding the animals implanted with fresh S912 CDT, 12 out of 16 animals were studied with CE-MRI. It was observed that 7 out of 8 animals had intact BBB during the initial mass development (average volume on day 28 p.i. $32\pm 9\text{ mm}^3$, $n=8$); 2 out of those 7 were also studied at the final stages of tumour development (average volume on days 39 and 48 p.i. $136\pm 33\text{ mm}^3$) and displayed compromised BBB (Supplementary Figures 5 and 6). The remaining 4 animals had compromised BBB at an average tumour volume of $144\pm 57\text{ mm}^3$ (between days 40-48 p.i.).

For mice implanted with frozen CDT ($n=29$), animals were studied at the initial stages of mass development (average volume between day 21 and 30 p.i. $23\pm 14\text{ mm}^3$, $n=27$); 22 of them displayed compromised BBB, while for 5 mice, all from the 'short latency' group, the BBB was intact (average tumour volumes were $22\pm 13\text{ mm}^3$ and $25\pm 23\text{ mm}^3$, respectively), but no follow-up CE-MRI was acquired. The remaining 2 animals died before the CE-MRI exploration, therefore their BBB status was unknown.

In the last batch of mice implanted with CDT obtained from a frozen S912 tumour piece, 3 out of 9 animals had intact BBB (average volume at the CE-MRI exploration $25\pm 3\text{ mm}^3$), but no follow-up explorations were performed. The masses with compromised BBB ($n=6$) were on average $33\pm 31\text{ mm}^3$ tumour volume.

MRS

The average spectra for tumours from each group of mice at short and long TE can be seen in Supplementary Figures 7 and 8, while average peak height ratios at both TEs analysed for animals implanted with CDT are presented in Supplementary Tables 4 and 5. In the latter it can be seen that SL 40 p.i. compared to the day 18 p.i. tumours, there was a statistically significant increase of Cho/Cr and ML/Cr ratios, suggesting progression to a more aggressive status, while comparing SL tumours at day 18 and 21 p.i., these changes were not so apparent. These pattern differences were also evident amongst tumours derived from fresh S912 CDT (grade III tumours, see histopathology results section) and those derived from frozen S912 CDT or CDT obtained from frozen S912 tumour (WHO grade IV tumours, as it will be reported in histopathology section).

MRSI

Apart from PE-MRSI using DMSO, the spectral pattern of GEM was also perturbed with hyperglycaemia to produce maps of D-glucose (at SET) or lactate (at LET) accumulation as in [3]. Supplementary Figure 9 shows the mentioned maps for the the animal G6-S912 (belonging to the ‘short latency’ group with PE-MRSI using DMSO previously presented in Figure 2). The "glucose accumulation" map suggests a strong heterogeneity of glucose arrival /consumption within the tumour.

Histopathology Studies

Grade III anaplastic ODG displayed a solid growth pattern composed of polygonal cells with pleomorphic nuclei corresponding to a medium grade of anisokaryosis. The tumour cells presented an evident eosinophilic and poorly delimited cytoplasm. Mitotic cells were evident. Moreover, some cells displayed picnotic nuclei, but clear necrotic foci were not observed. Proliferative capillaries and glomeruloid vessels together with multifocal bleedings were present. Furthermore, tumour cells also infiltrated surrounding nervous tissue.

OA presented oligodendrocytes (expressing Olig2) and astrocytes (expressing GFAP) intimately mixed in a solid growth pattern. They showed histological features of malignancy (increased cellularity, anisokariosis, pleomorphism and increased mitotic activity). Tumour cells infiltrated surrounding nervous tissue.

The growth pattern of GBM was also solid and the tumour was formed by polygonal cells with basophilic loose chromatin nuclei that showed a high grade of anisokaryosis. In this tumour type, mitotic cells were abundant and more evident than in the other tumours. The tumour also showed an abundant diffuse basophilic secretion throughout the whole mass. Typical pseudopalisading necrotic areas characteristic of GBM were present. Adjacent nervous tissue was generally compressed by the tumour, but focally infiltrated by neoplastic cells.

Genotype check

Nine randomly chosen animals with implanted CDT had the genotype of their tumours checked in order to confirm the accordance with the original genotype. All tumours checked presented the expected transgene (Tg; S100B-v-erbB) as in the initial S912 mouse. However, three of the analysed masses presented loss of heterozygosity for the knockout gene (Ink4a-Arf (+/-)), being homozygotic (KO-/-). Two of these animals belonged to the group implanted with fresh CDT (‘short latency’ group) while one belonged to the ‘intermediate latency’ group, from the batch of mice injected with frozen CDT.

SUPPLEMENTARY DISCUSSION

Genotype check

Considering the genotyping of random animals, three animals out of nine presented loss of heterozygosity for Ink4a-Arf. The homozygous deletion of Ink4a-Arf in humans is often associated with malignant progression in high-grade gliomas [12,13] being also one of the most frequent mutations found in human gliomas [14,15] associated with short survival times [12]. In transgenic mice it has been described that animals homozygous for loss of Ink4a-Arf, develop tumours with similar incidence, but with decreased latency and survival in comparison to heterozygous animals [10]. In our studies, the phenotypic consequences for the loss of heterozygosity for the original S912 knockout were not obvious, as the animals with homozygous deletion fell both into the ‘short latency’ and ‘intermediate latency’ groups. However, this genomic difference is not negligible and should be taken into account in future studies, possibly using a wider gene sequencing approach.

Non-invasive MR monitoring of S912-derived tumours

Regarding MRI/MRS/MRSI acquisition of S912-derived tumours, this allowed preliminary *in vivo* assessment of their grade, later confirmed by histopathological analysis. Tumours developed from fresh S912 CDT showed features associated with low/intermediate grade glioma (Supplementary Figure 7), i.e. increased Cho/Cr ratio, decrease in NAA which is usually associated with a decrease of viable neurons [16-18], and increased lactate signal and detection of mobile lipids [18,19]; while patterns of tumours derived from frozen S912 CDT (Supplementary Figure 8) have clearly higher lactate and mobile lipids peaks usually associated with GBM [8]. Additionally, still regarding tumours derived from frozen CDT, the decrease in the estimated mI/Gly ratio [20] for intermediate and long latency groups with respect to short latency group (Supplementary Table 4) could suggest a metabolic subtype. This decrease is not so clear in case of tumours derived from fresh S912 CDT and further *ex vivo* and *in vitro* extract studies would be needed to clarify it. Although a detailed *in vivo* analysis of the MRS pattern of GBM subtypes is still lacking, *ex vivo* data obtained by HR-MAS analyses of tumour biopsies suggests that human secondary GBM could display a much higher mI content than primary ones [21].

Besides, other MR studies performed could also help in the non-invasive characterization of the GEM-derived transplantable tumours. CE-MRI allowed assessment of the state of BBB integrity and a qualitative orientation of a possible transition to higher grade. Mice implanted with fresh S912 CDT studied at the initial stages of tumour development (average volume $32 \pm 9 \text{ mm}^3$) had mostly intact BBB (7 out of 8). When CE-MRI was repeated for 2 of these tumours at the longer growth time (average volume

136±33mm³), they displayed contrast intake (Supplementary Figure 5 and 6), which suggested an undergoing transition of grade III to a higher grade IV. The progression in the tumour grade was more evident for tumours derived from frozen samples as the BBB was compromised at earlier stages (22±13 mm³) in 22 out of 27 animals investigated by CE-MRI.

REFERENCES FOR SUPPLEMENTARY MATERIAL

1. Ernst T, Hennig J (1995) Improved water suppression for localized in vivo ¹H spectroscopy. *J Magn Reson B* 106 (2):181-186
2. Delgado-Goni T, Martin-Sitjar J, Simoes RV, Acosta M, Lope-Piedrafita S, Arus C (2013) Dimethyl sulfoxide (DMSO) as a potential contrast agent for brain tumors. *NMR Biomed* 26 (2):173-184. doi:10.1002/nbm.2832
3. Simoes RV, Delgado-Goni T, Lope-Piedrafita S, Arus C (2010) ¹H-MRSI pattern perturbation in a mouse glioma: the effects of acute hyperglycemia and moderate hypothermia. *NMR Biomed* 23 (1):23-33. doi:10.1002/nbm.1421
4. Mehrara E, Forssell-Aronsson E, Ahlman H, Bernhardt P (2007) Specific growth rate versus doubling time for quantitative characterization of tumor growth rate. *Cancer research* 67 (8):3970-3975. doi:10.1158/0008-5472.CAN-06-3822
5. Simoes RV, Garcia-Martin ML, Cerdan S, Arus C (2008) Perturbation of mouse glioma MRS pattern by induced acute hyperglycemia. *NMR Biomed* 21 (3):251-264. doi:10.1002/nbm.1188
6. <http://gabrmn.uab.es/DMPM>. Last accessed: 28/12/2015.
7. Ortega-Martorell S, Olier I, Julia-Sape M, Arus C (2010) SpectraClassifier 1.0: a user friendly, automated MRS-based classifier-development system. *BMC bioinformatics* 11:106. doi:1471-2105-11-106 [pii] 10.1186/1471-2105-11-106
8. Simoes RV, Ortega-Martorell S, Delgado-Goni T, Le Fur Y, Pumarola M, Candiota AP, Martin J, Stoyanova R, Cozzone PJ, Julia-Sape M, Arus C (2012) Improving the classification of brain tumors in mice with perturbation enhanced (PE)-MRSI. *Integrative biology : quantitative biosciences from nano to macro* 4 (2):183-191. doi:10.1039/c2ib00079b
9. Louis DN, Ohgaki H, Wiestler OD, Cavenee WK, Burger PC, Jouvet A, Scheithauer BW, Kleihues P (2007) The 2007 WHO classification of tumours of the central nervous system. *Acta Neuropathol* 114 (2):97-109. doi:10.1007/s00401-007-0243-4
10. Weiss WA, Burns MJ, Hackett C, Aldape K, Hill JR, Kuriyama H, Kuriyama N, Milshteyn N, Roberts T, Wendland MF, DePinho R, Israel MA (2003) Genetic determinants of malignancy in a mouse model for oligodendroglioma. *Cancer research* 63 (7):1589-1595
11. Delgado-Goni T, Julia-Sape M, Candiota AP, Pumarola M, Arus C (2014) Molecular imaging coupled to pattern recognition distinguishes response to temozolomide in preclinical glioblastoma. *NMR Biomed* 27 (11):1333-1345. doi:10.1002/nbm.3194
12. Cairncross JG, Ueki K, Zlatescu MC, Lisle DK, Finkelstein DM, Hammond RR, Silver JS, Stark PC, Macdonald DR, Ino Y, Ramsay DA, Louis DN (1998) Specific genetic predictors of chemotherapeutic response and survival in patients with anaplastic oligodendrogliomas. *Journal of the National Cancer Institute* 90 (19):1473-1479
13. Bigner SH, Rasheed BK, Wiltshire R, McLendon RE (1999) Morphologic and molecular genetic aspects of oligodendroglial neoplasms. *Neuro-oncology* 1 (1):52-60
14. Jen J, Harper JW, Bigner SH, Bigner DD, Papadopoulos N, Markowitz S, Willson JK, Kinzler KW, Vogelstein B (1994) Deletion of p16 and p15 genes in brain tumors. *Cancer research* 54 (24):6353-6358
15. Schmidt EE, Ichimura K, Reifenberger G, Collins VP (1994) CDKN2 (p16/MTS1) gene deletion or CDK4 amplification occurs in the majority of glioblastomas. *Cancer research* 54 (24):6321-6324
16. Cha S (2003) Perfusion MR imaging: basic principles and clinical applications. *Magnetic resonance imaging clinics of North America* 11 (3):403-413
17. Law M, Yang S, Wang H, Babb JS, Johnson G, Cha S, Knopp EA, Zagzag D (2003) Glioma grading: sensitivity, specificity, and predictive values of perfusion MR imaging and proton MR spectroscopic imaging compared with conventional MR imaging. *AJNR American journal of neuroradiology* 24 (10):1989-1998
18. Price SJ (2007) The role of advanced MR imaging in understanding brain tumour pathology. *British journal of neurosurgery* 21 (6):562-575. doi:10.1080/02688690701700935

19. Jenkinson MD, Du Plessis DG, Walker C, Smith TS (2007) Advanced MRI in the management of adult gliomas. *British journal of neurosurgery* 21 (6):550-561.
doi:10.1080/02688690701642020
20. Candiota AP, Majos C, Julia-Sape M, Cabanas M, Acebes JJ, Moreno-Torres A, Griffiths JR, Arus C (2011) Non-invasive grading of astrocytic tumours from the relative contents of myo-inositol and glycine measured by in vivo MRS. *JBR-BTR : organe de la Societe royale belge de radiologie* 94 (6):319-329
21. Martinez-Bisbal MC, Marti-Bonmati L, Piquer J, Revert A, Ferrer P, Llacer JL, Piotta M, Assemat O, Celda B (2004) ¹H and ¹³C HR-MAS spectroscopy of intact biopsy samples ex vivo and in vivo ¹H MRS study of human high grade gliomas. *NMR Biomed* 17 (4):191-205.
doi:10.1002/nbm.888

SUPPLEMENTARY TABLES

Supplementary Table 1 Distribution of experimental animals depending on the source of cells used for each tumour generation protocol, and identifiers of animals in each group

| <i>Group</i> | <i>No. of animals</i> | <i>Source of cells for tumour generation</i> | <i>Alphanumeric identifier of animals in the group</i> |
|--------------|-----------------------|--|--|
| A | 6 | Standard GL261 cells | C(unique number) |
| B | 6 | CDT cultured from fresh GL261 tumour | |
| C | 7 | CDT cultured from frozen GL261 tumour | |
| D | 29 | CDT cultured from fresh S912 tumour | G(unique number)-S912 |
| E | 29 | Frozen CDT cultured from fresh S912 tumour | Gc(unique number)-S912 |
| F | 9 | CDT cultured from frozen S912 tumour | Gtc(unique number)-S912 |

Supplementary Table 2 Survival time (days, mean \pm SD) of each experimental group of mice. There was a significant difference detected between tumours derived from S912 CDT and tumours derived from GL261 CDT (*) and between either intermediate or long latency tumours derived from frozen S912 CDT and tumours derived from fresh S912 CDT (**). The difference in survival time was non-significant between tumours derived from GL261 CDT (either fresh or frozen) and standard GL261 tumour, and neither between tumours derived from S912 CDT cultured from a frozen piece of tumour and tumours derived from fresh S912 CDT

| Group of animals | GL261 tumours (n=6) | GL261 CDT | | S912 CDT | | | | | |
|----------------------|---------------------|--------------|---------------------|---------------------|----------------------------|----------------------|----------------------------|---------------------|--------------------------|
| | | | | From fresh tumour | | | | | From frozen tumour (n=9) |
| | | | | Fresh CDT | | Frozen CDT | | | |
| | | Fresh (n=6) | Frozen tumour (n=7) | Short latency (n=9) | Intermediate latency (n=7) | Short latency (n=13) | Intermediate latency (n=9) | Long latency (n=5) | |
| Mean survival (days) | 19 \pm 2.9 | 23 \pm 2.5 | 25 \pm 2.4 | 40 * \pm 4.9 | 61 * \pm 20.6 | 41* \pm 10.6 | 103 */** \pm 42.4 | 163*/** \pm 124.2 | 45* \pm 15.3 |

Supplementary Table 3 Average metabolite peak height ratios at both short and long TE from UL2 normalized spectra for tumours generated from fresh S912 CDT: ‘short latency’ (SL) group at day 18, 21 and 40 p.i. and ‘intermediate latency’ (IL) group 35-42 days p.i.; standard GL261 tumours 11 p.i. and normal brain parenchyma (NB) of C57BL/6 mice. The main resonances, used for ratio calculations are labelled as follows: Cho (choline containing compounds) at 3.21 ppm; Cr (total creatine) at 3.03 ppm; mL-Gly (myo-inositol + glycine) at SET or Gly (mostly glycine at LET [20]) at 1.32 ppm; ML (mobile lipids and/or macromolecules) at 1.28 ppm; NAA (N-acetylaspartate) at 2 ppm; Tau (taurine) at 3.42 ppm. SET:(mL+Gly)/Cr / LET:Gly/Cr approximates the mL/Gly ratio in the intact tissue [20]. Significant differences for peak height ratios between SL day 21, SL day 40 and IL in comparison to SL day 18 are marked with [^]; significant difference between SL day 18, SL day 21, SL day 40 and IL in comparison to standard GL261 are marked with [§] and in comparison to NB are marked with [^]; and significant differences between standard GL261 and NB are marked with [&]. See also references [8,2,3] for further details about resonance assignment

| | SL (n=9) day 18 | | SL (n=9) day 21 | | SL (n=7) day 40 | | IL (n=5) day 35-42 | | GL261 (n=12) day 11 | | NB (n=4) | | |
|---------------------------------|--------------------|--------------------|--------------------|---------------------|--------------------|---------------------|-----------------------|---------------------|------------------------|-----------------------|----------|------|------|
| | Average | SD | Average | SD | Average | SD | Average | SD | Average | SD | Average | SD | |
| SET | Cho/Cr | 1.35 ^{§^} | 0.09 | 1.40 [^] | 0.11 | 1.80 ^{^*} | 0.25 | 1.92 [*] | 0.40 | 1.43 ^{&} | 0.25 | 0.98 | 0.03 |
| | ML/Cr | 0.90 ^{§^} | 0.12 | 0.81 | 0.21 | 1.38 ^{§^*} | 0.37 | 2.47 ^{§^*} | 3.86 | 1.68 ^{&} | 0.73 | 0.56 | 0.24 |
| | NAA/Cr | 1.06 | 0.11 | 1.02 | 0.24 | 0.97 | 0.12 | 1.38 | 3.00 | 1.10 | 0.30 | 1.01 | 0.06 |
| LET | (mL+Gly)/Cr | 0.66 [^] | 0.80 | 0.71 [^] | 0.60 | 1.29 ^{§^*} | 0.15 | 1.21 ^{§^*} | 0.09 | 0.75 ^{&} | 0.23 | 0.39 | 0.04 |
| | Cho/Cr | 1.47 [§] | 0.32 | 1.78 ^{§^*} | 0.27 | 2.30 ^{§^*} | 0.50 | 3.02 [^] | 1.96 | 3.07 ^{&} | 0.94 | 1.14 | 0.06 |
| | Lac/Tau | 0.76 [§] | 0.28 | 0.91 [§] | 0.24 | 1.11 [§] | 0.82 | 2.85 [^] | 2.29 | 3.21 ^{&} | 1.61 | 0.87 | 0.51 |
| SET:(mL+Gly)/Cr / LET:Gly/Cr | NAA/Cr | 0.71 [^] | 0.13 | 0.64 [^] | 0.15 | 0.50 [^] | 0.20 | 0.96 | 0.78 | 0.79 | 0.33 | 1.01 | 0.04 |
| | Gly/Cr | 0.22 [§] | 0.08 | 0.27 [§] | 0.09 | 0.67 ^{§^*} | 0.32 | 0.84 ^{§^*} | 0.44 | 1.55 ^{&} | 0.23 | 0.17 | 0.07 |
| | | 3.49 [§] | 2.26 | 2.87 [§] | 0.86 | 2.34 [§] | 1.31 | 3.41 [§] | 1.79 | 0.45 ^{&} | 0.21 | 2.88 | 1.73 |

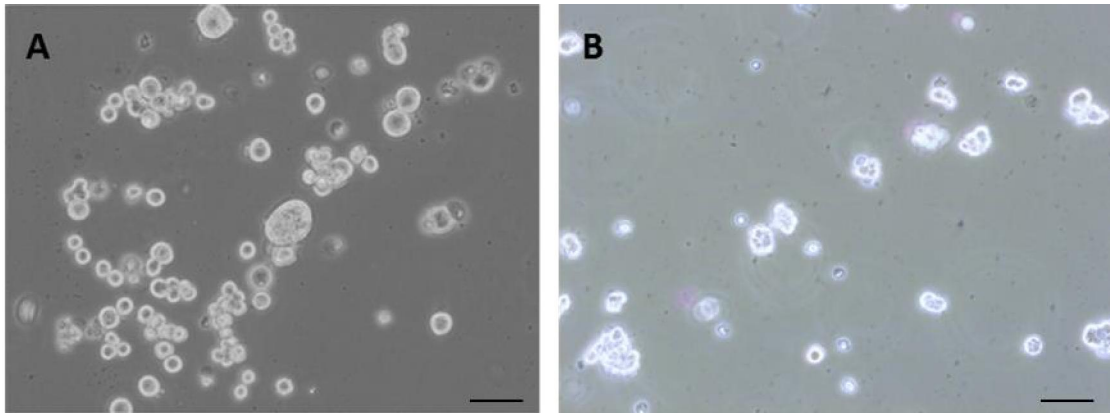
Supplementary Table 4 Average metabolite peak height ratios at both short and long TE from UL2 normalized spectra for tumours generated with frozen S912 CDT: ‘short latency’ (SL) group, ‘intermediate latency’ (IL) group and ‘long latency’ (LL); tumours generated from S912 CDT obtained from frozen tumour (FT) and normal brain parenchyma (NB) of C57BL/6 mice. The main resonances, used for ratio calculations are labelled as follows: Cho (choline containing compounds) at 3.21 ppm; Cr (total creatine) at 3.03 ppm; mL-Gly (myo-inositol + glycine) at SET or Gly (mostly glycine at LET [20]) at 3.55 ppm; Lac (lactate) at 1.32 ppm; ML (mobile lipids and/or macromolecules) at 1.28 ppm; NAA (N-acetylaspartate) at 2 ppm, Tau (taurine) at 3.42 ppm. SET:(mL+Gly)/Cr / LET:Gly/Cr approximates the mL/Gly content in the intact tissue [20]. Significant difference for peak ratios between IL, LL and FT in comparison to SL are marked with [^]; significant differences between SL, LL, LL and FT in comparison to GL261 and NB are marked with ^s and ^{*}, respectively; and significant differences between standard GL261 and NB are marked with [&]

| | SL (n=13) | | IL (n=9) | | LL (n=7) | | FT (n=5) | | GL261 (n=12) day 11 | | NB (n=4) | | | |
|---------------------------------|--------------------|--------------------|---------------------|---------------------|--------------------|---------------------|---------------------|---------------------|------------------------|-----------------------|-----------------------|------|------|------|
| | Average | SD | Average | SD | Average | SD | Average | SD | Average | SD | Average | SD | | |
| SET | Cho/Cr | 1.40 [*] | 0.27 | 2.15 ^{^s*} | 0.31 | 0.46 | 1.45 [*] | 0.77 | 1.63 [*] | 0.77 | 1.43 ^{&} | 0.25 | 0.98 | 0.03 |
| | ML/Cr | 1.30 [*] | 0.53 | 8.43 ^{^s*} | 2.86 | 2.77 ^{^s*} | 1.85 | 3.54 ^{^s*} | 2.46 | 1.68 ^{&} | 0.73 | 0.56 | 0.24 | |
| | NAA/Cr | 1.15 | 0.22 | 2.37 ^{^*} | 0.78 | 1.39 | 0.77 | 1.46 | 0.37 | 1.10 | 0.30 | 1.01 | 0.06 | |
| | (mL+Gly)/Cr | 0.81 | 0.26 | 1.62 ^{^s*} | 0.37 | 0.98 | 0.57 | 1.33 ^{^*} | 0.36 | 0.75 ^{&} | 0.23 | 0.39 | 0.04 | |
| LET | Cho/Cr | 1.46 ^s | 0.23 | 3.13 ^{^*} | 0.44 | 4.58 ^{^*} | 4.29 | 2.89 ^{^*} | 0.98 | 3.07 ^{&} | 0.94 | 1.14 | 0.06 | |
| | Lac/Tau | 1.62 ^{s*} | 0.47 | 7.84 ^{^s*} | 6.16 | 1.81 | 1.01 | 3.23 ^{^*} | 1.94 | 3.21 ^{&} | 1.61 | 0.87 | 0.51 | |
| | NAA/Cr | 0.69 | 0.11 | 1.48 ^{^s} | 1.00 | 1.87 ^s | 1.82 | 0.58 | 0.23 | 0.79 | 0.33 | 1.01 | 0.04 | |
| Gly/Cr | 0.23 ^s | 0.10 | 1.25 ^{^*} | 0.39 | 1.92 ^{^*} | 2.57 | 1.08 ^{^*} | 0.71 | 1.55 ^{&} | 0.23 | 0.17 | 0.07 | | |
| SET:(mL+Gly)/Cr / LET:Gly/Cr | 3.66 ^{s*} | 1.38 | 1.36 ^{^s*} | 0.36 | 0.36 [^] | 0.02 | 1.61 ^{^s*} | 0.73 | 0.45 ^{&} | 0.21 | 2.88 | 1.73 | | |

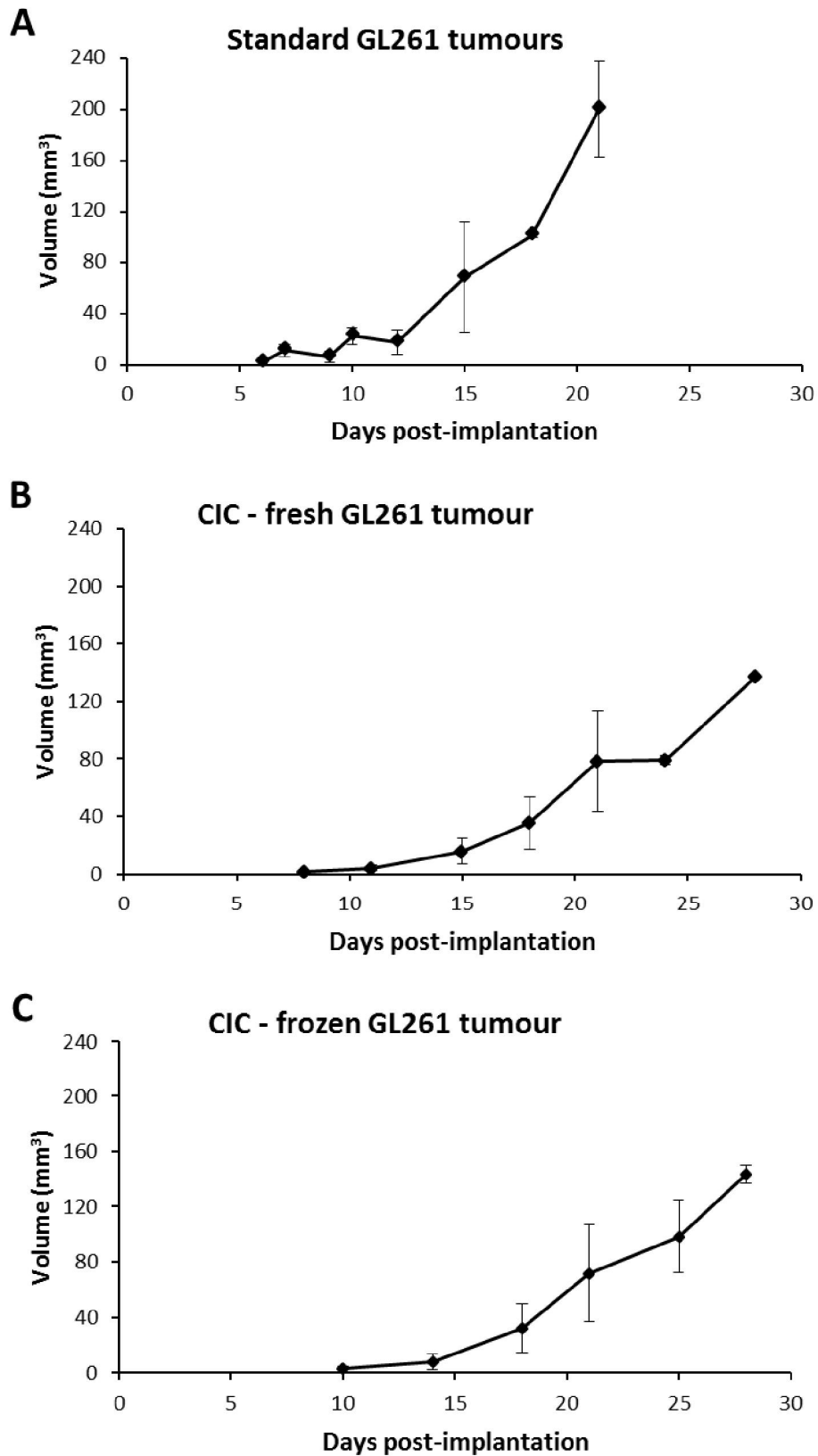
Supplementary Table 5 Number of animals/PE-MRSI explorations carried out

| Group of animals | PE-MRSI with DMSO | PE-MRSI with glucose in hypothermia |
|------------------|-------------------|-------------------------------------|
| Group D | 11 | 7 |
| Group E | 18 | 14 |
| Group F | 4 | 4 |

SUPPLEMENTARY FIGURES



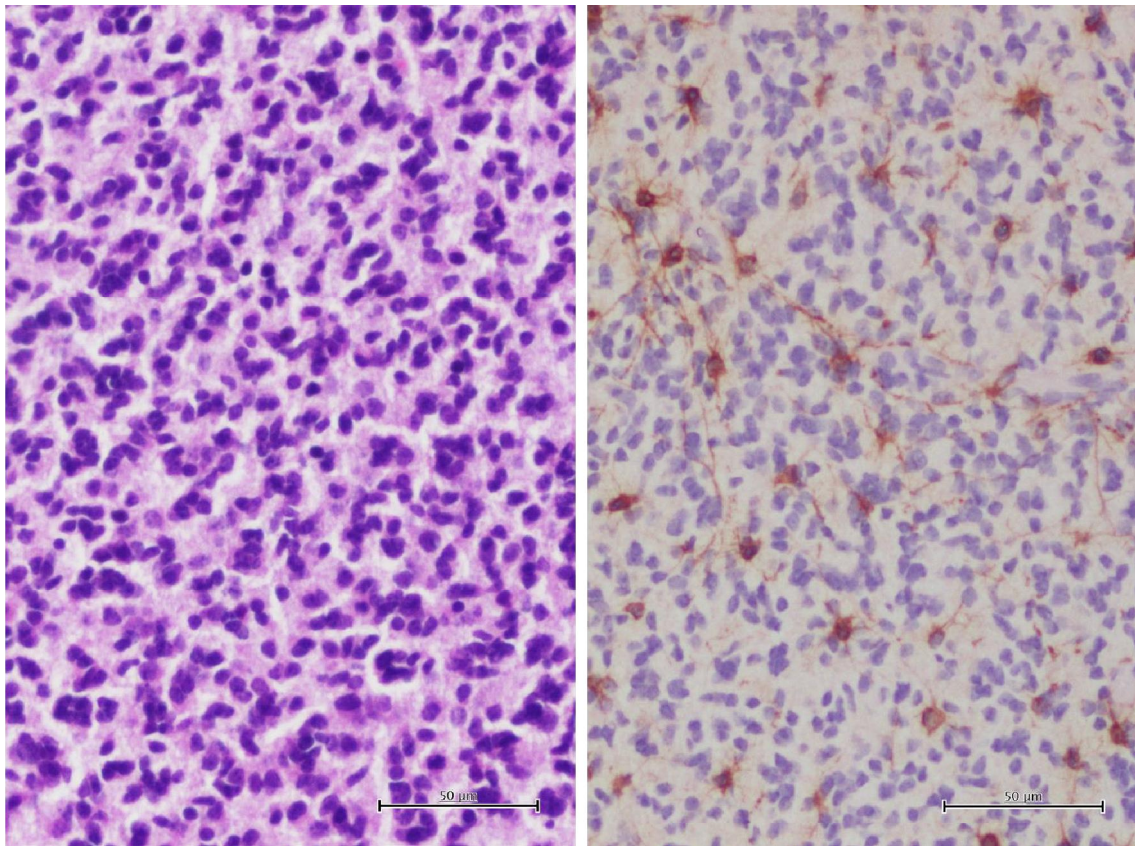
Supplementary Fig. 1 Microscope image of CDT aggregates generated from a fresh piece of **A)** GL261 tumour and **B)** S912GEM tumour after 17 days of culture. Scale bar; 100 μm



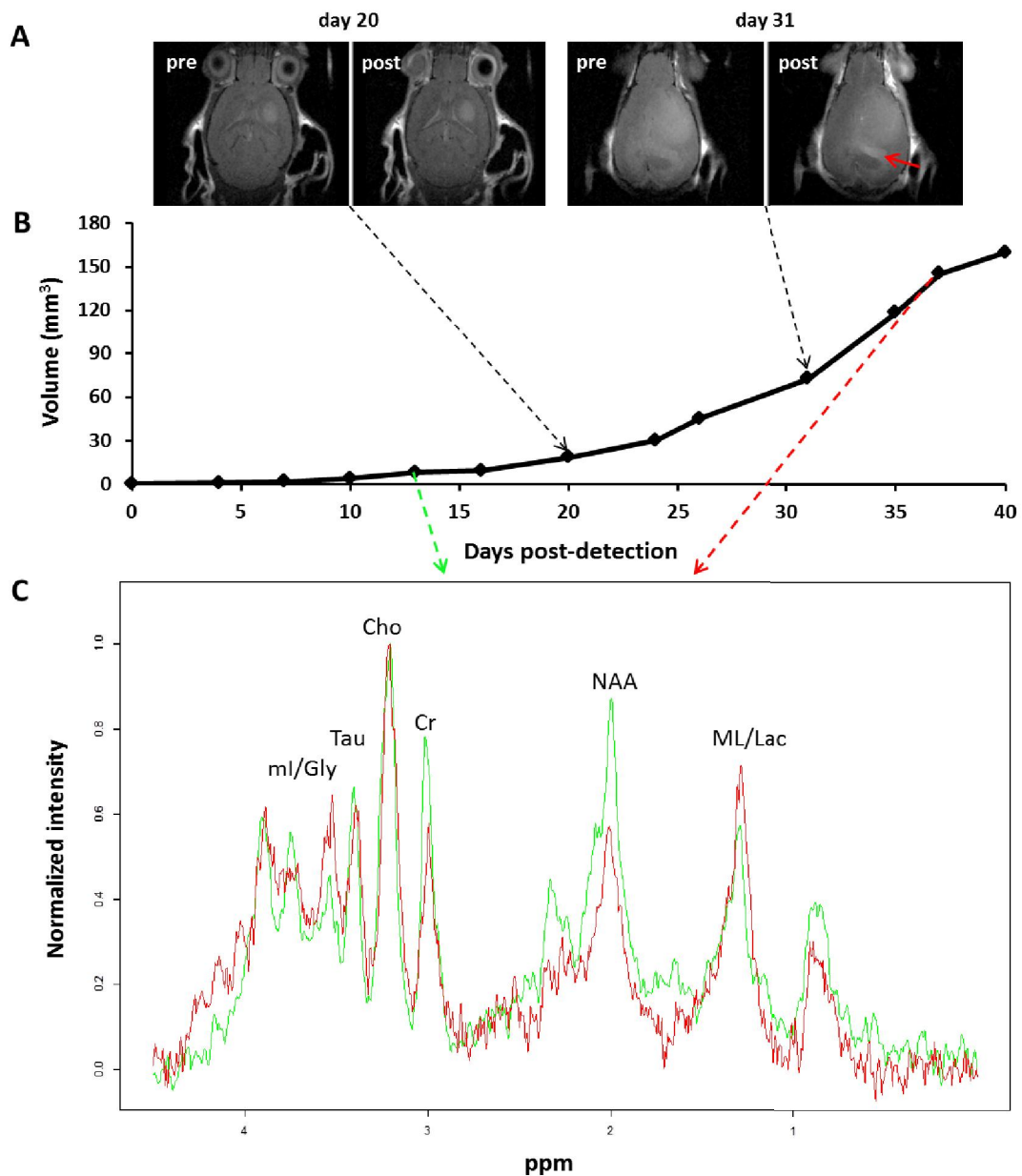
Supplementary Fig. 2 Average growth curves representing the mean \pm SD (vertical bars) of tumour volumes grown from implanted: A) GL261 cells (n=6); B) CDT cultured from fresh GL261 tumour (n=6), C) CDT cultured from frozen GL261 tumour (n=7). Bars state \pm SD of volume at each time point of volume measurement



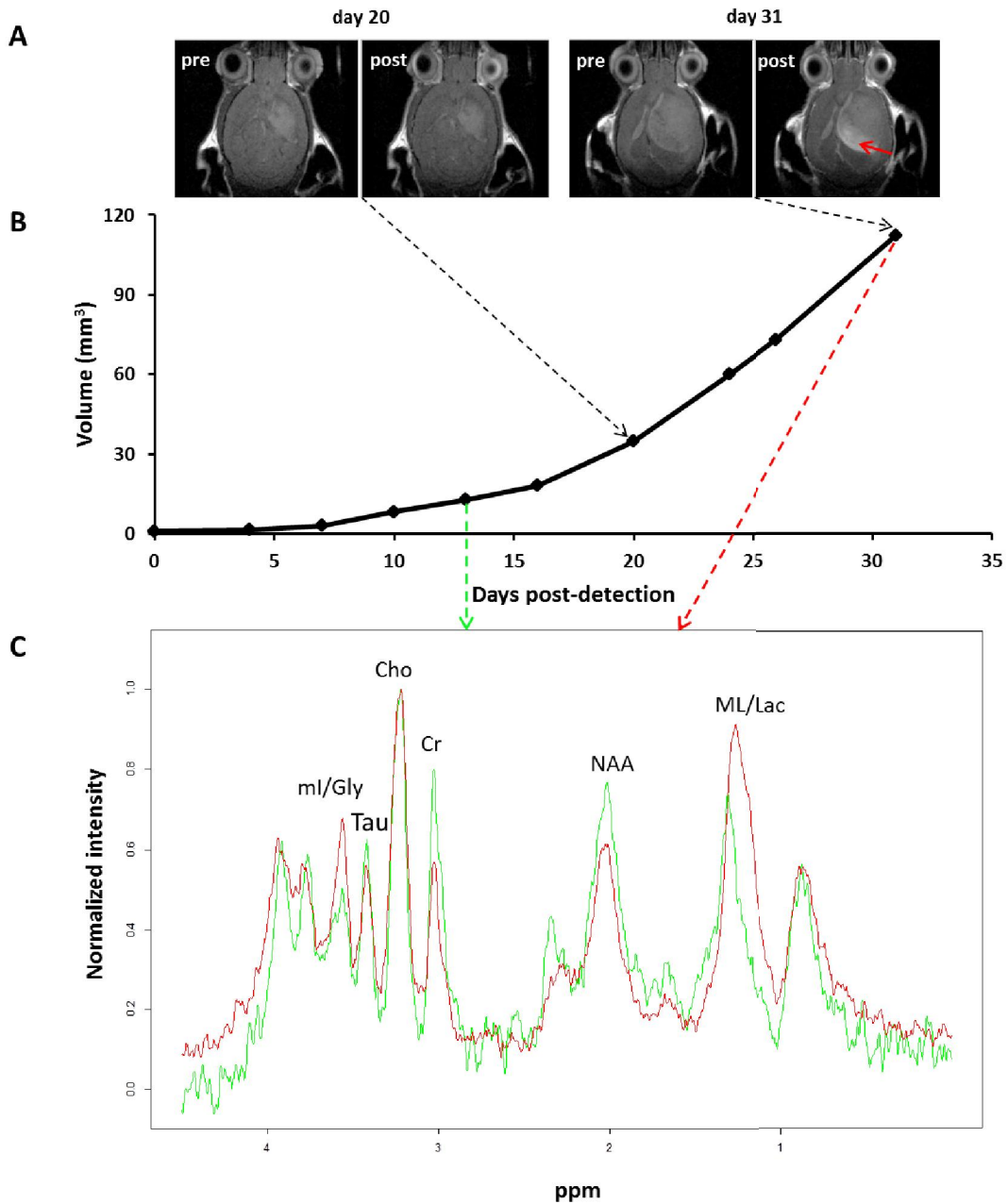
Supplementary Fig. 3 Coronal T_{1W} MRI of the S912 mouse brain **A)** pre- and **B)** post-contrast administration, as well as **C)** subtraction of the two previous images, acquired at 7T 32 days after initial tumour detection. The black arrow in C indicates the area of contrast enhancement



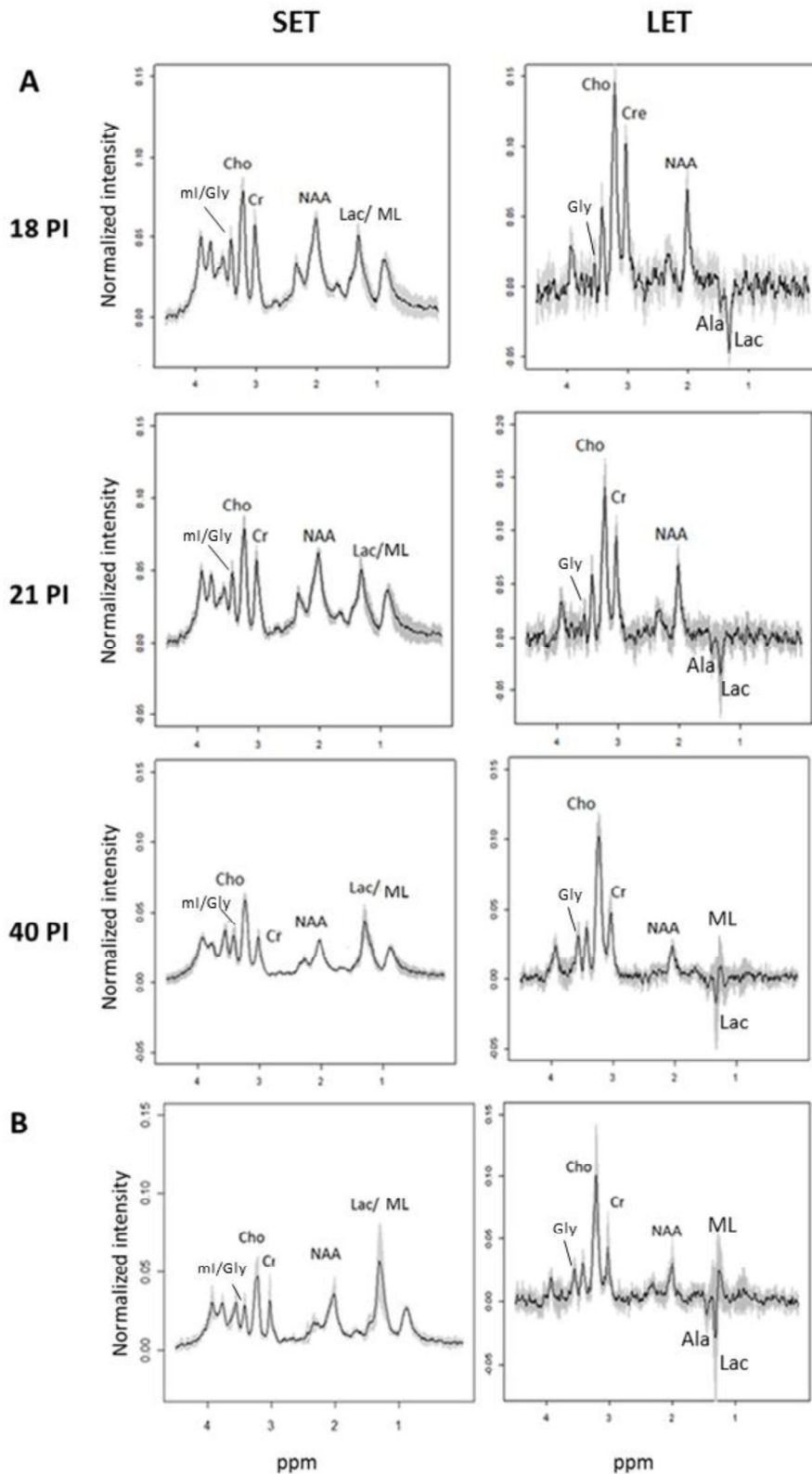
Supplementary Fig. 4 Hematoxylin and eosin stained (left side) and glial fibrillary acidic protein (GFAP) immunohistochemically stained (right side) characteristic paraffin sections of the S912 anaplastic oligodendroglioma tumour of WHO grade III. The neoplastic sample displays a solid growth pattern composed of polygonal cells with pleomorphic basophilic nuclei (corresponding to a medium grade of anisokaryosis) and an evident and poorly delimited eosinophilic cytoplasm. Moreover, some cells display picnotic nuclei. Immunohistochemical analysis is characterized by low levels of GFAP expression confined to reactive astrocytes (brown colour), mixed with immunonegative neoplastic cells (original magnification x200), bar 50µm.



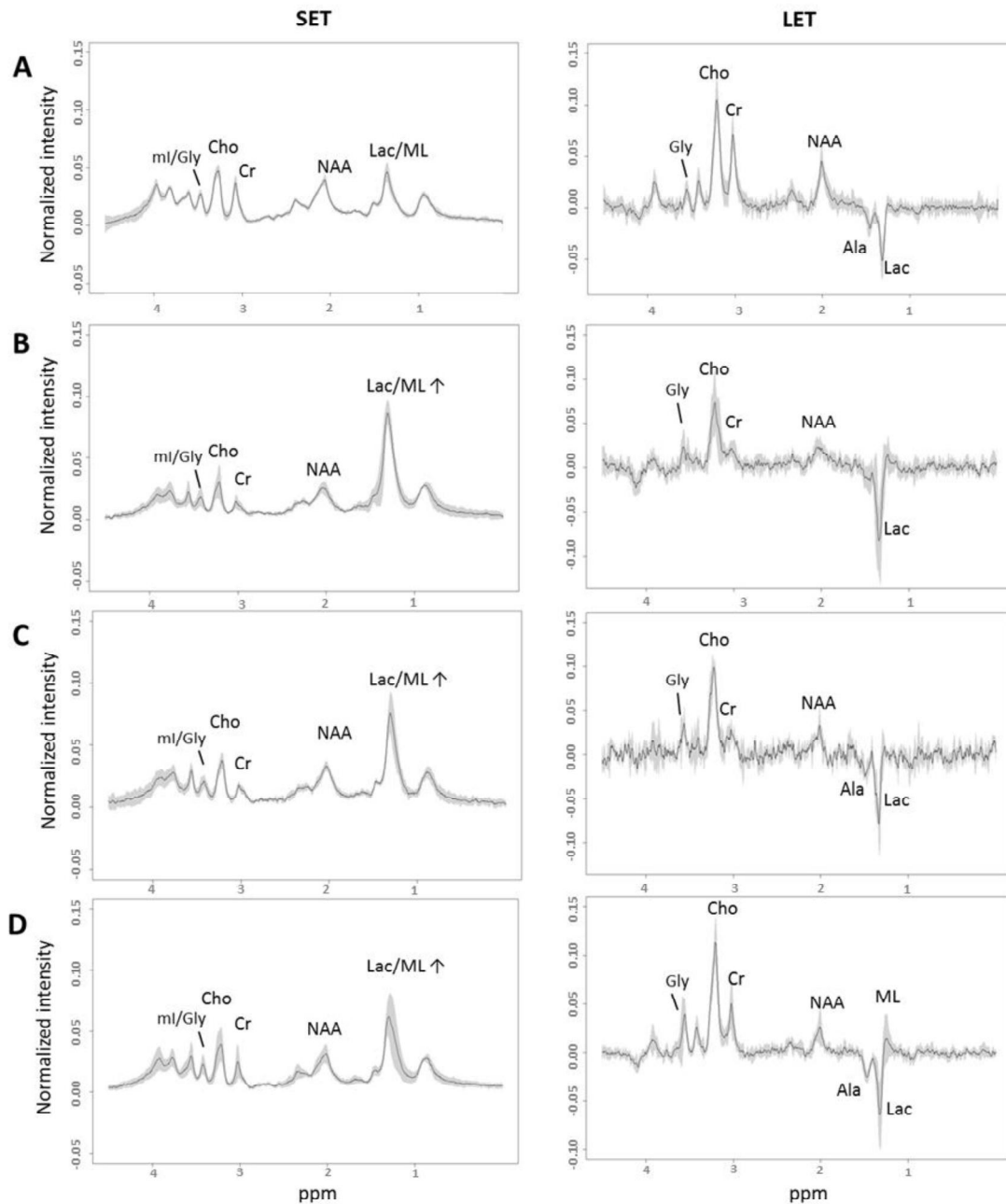
Supplementary Fig. 5 Changes in contrast uptake and spectral pattern of G4-S912 tumour during its growth. **A**) Coronal T_{1W} MRI pre and post CE at day 20 p.i. (left) and at day 31 p.i. (right). The red arrow indicates the zone of contrast uptake. **B**) Growth curve of the tumour. Black arrows indicate time points of the CE studies; while green and red arrows show time points at which SV MR spectra presented in **C**) were acquired. **C**) Comparison of the spectra acquired at short TE (12 ms) at initial (red) and final (red) stages of tumour progression. Cho: choline containing compounds, Cr: total creatine, ml/Gly: myo-inositol/glycine, NAA: N-acetylaspartate, Lac: lactate, ML: mobile lipids, Tau: taurine



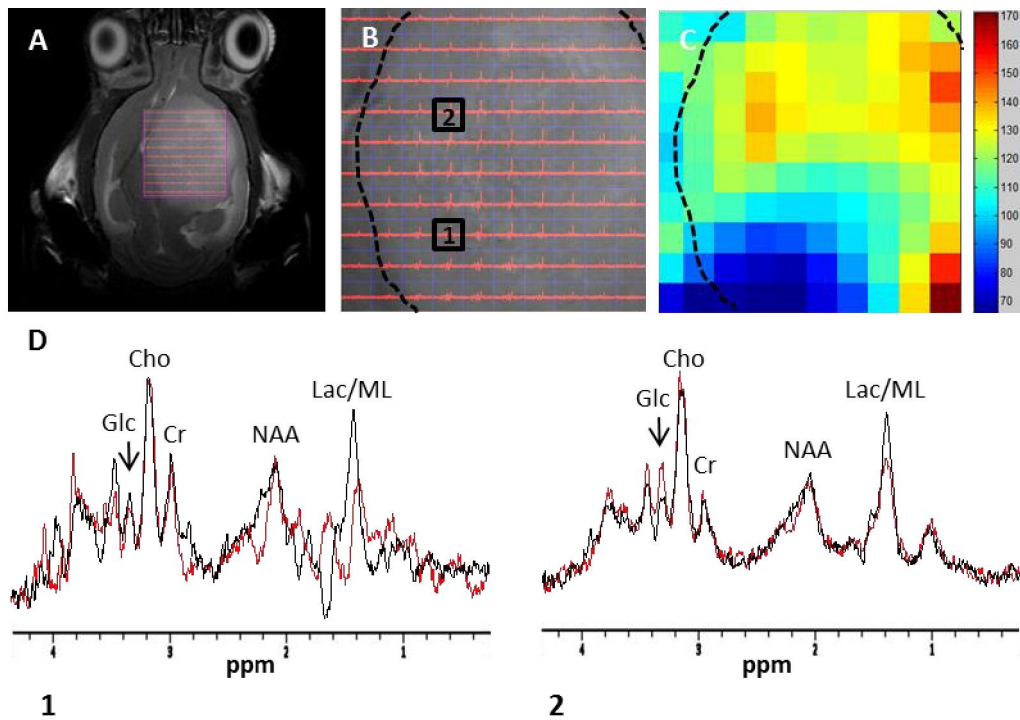
Supplementary Fig. 6 Changes in contrast uptake and spectral pattern of G5-S912 tumour during its growth. **A)** Coronal T_{1W} MRI pre and post CE at day 20 p.i. (left) and 31 p.i. The red arrow indicates the zone of contrast uptake. **B)** Growth curve of the tumour. Black arrows indicate time points of the CE studies; while green and red arrows show time points at which SV MR spectra presented in C) were acquired. **C)** Comparison of the spectra acquired at short TE (12 ms) at initial (red) and final (red) stages of tumour progression. Cho: choline containing compounds, Cr: creatine, ml/Gly: myo-inositol/glycine, NAA: N-acetylaspartate, Lac: lactate, ML: mobile lipids, Tau: taurine



Supplementary Fig. 7 Average UL2 normalized SV MR spectra (\pm SD, grey shading) at short (12 ms) and long (136 ms) TE obtained from $(1.5 - 3.0 \text{ mm})^3$ voxels of tumours generated from GEM S912 fresh CDT of: **A** ‘short latency’ group of animals ($n=25$) acquired at day 18 ($n=9$), 21 ($n=9$) and 40 ($n=7$) p.i. and of **B** ‘intermediate latency’ group of animals ($n=5$) acquired between days 35 and 42 p.i. Ala: Alanine, Cho: choline containing compounds, Cr: total creatine, Gly: glycine, Lac: lactate, ml: myo-inositol, ML: mobile lipids, NAA: N-acetylaspartate



Supplementary Fig. 8 Average UL2 normalized SV MR spectra (\pm SD, grey shading) at short (12 ms) and long (136 ms) TE obtained from tumours generated from frozen GEM S912 CDT (A, B, C) and tumours generated from CDT obtained from a frozen piece of GEM S912 tumour (D): **A**) ‘short latency’ group of animals (n=13), SV acquired between days 21 and 34 p.i., **B**) ‘intermediate latency’ group of animals (n=6), SV acquired between days 59 and 77 p.i., **C**) ‘long latency’ group of animals (n=4), SV acquired between days 86 and 253 p.i., **D**) group of animals implanted with CDT obtained from a frozen tumour (n=8), SV acquired between day 26 and 80 p.i. Ala: alanine, Cho: choline containing compounds, Cr: total creatine, Gly: glycine, Lac: lactate, ml: myo-inositol, ML: mobile lipids, NAA: N-acetylaspartate. Black arrows in B, C and D indicate visible Lac/ML increase in comparison to ‘short latency’ group (A)



Supplementary Fig. 9 Representative PE-MRSI with hyperglycaemia and hypothermia of the tumour in the animal G6-S912 acquired at 41 days p.i.: **A**) VOI superimposed with the reference image (T_{2W} MRI). **B**) Enlargement of VOI: black dotted line labels the tumoural mass and black squares 1 and 2 correspond to the individual voxels of the MRSI grid from which SV spectra were extracted and shown in D). **C**) Color-coded intensity map of D-glucose caused pattern increase at 3.43 ppm (14ms TE) acquired at 88 minutes after glucose administration. **D**) Spectra of labelled voxels in the matrix (black squares) before (black spectrum) and after (red spectrum) glucose administration. The black arrow indicates the transient D-glucose accumulation peak at 3.43 ppm (Glc). Cho: choline containing compounds, Cr: total creatine, Lac/ML: Lactate/mobile lipids, NAA: N-acetylaspartate

